BIOCHEMISTRY
including biophysical chemistry & molecular biology

Article

pubs.acs.org/biochemistry

Structural Characterization of Interactions between the Double-Stranded RNA-Binding Zinc Finger Protein JAZ and Nucleic Acids

Russell G. Burge,† Maria A. Martinez-Yamout, H. Jane Dyson,* and Peter E. Wright*

Department of Integrative Structural and Computational Biology and the Skaggs Institute for Chemical Biology, The Scripps Research Institute, La Jolla, California 92037, United States

Supporting Information

ABSTRACT: The interactions of the human double-stranded RNA-binding zinc finger protein JAZ with RNA or DNA were investigated using electrophoretic mobility-shift assays, isothermal calorimetry, and nuclear magnetic resonance spectroscopy. Consistent with previous reports, JAZ has very low affinity for duplex DNA or single-stranded RNA, but it binds preferentially to double-stranded RNA (dsRNA) with no detectable sequence specificity. The affinity of JAZ for dsRNA is unaffected by local structural features such as loops, overhangs, and bulges, provided a sufficient length of reasonably well-structured A-form RNA (about 18 bp for a single zinc finger) is present. Full-length JAZ contains four Cys_2His_2 zinc fingers (ZF1−4) and has the highest apparent affinity for dsRNA; two-finger constructs ZF12 and ZF23 have lower affinity, and ZF34 binds even more weakly. The fourth zinc finger, ZF4, has no measurable RNA-binding affinity. Single zinc finger constructs ZF1, ZF2, and ZF3 show evidence for multiple-site binding on the minimal RNA. Fitting of quantitative NMR titration and isothermal calorimetry data to a two-site binding model gave $K_{d1} \sim 10$ μM and $K_{d2} \sim 100$ μM. Models of JAZ−RNA complexes were generated using the high-ambiguity-driven biomolecular docking (HADDOCK) program. Single zinc fingers bind to the RNA backbone without sequence specificity, forming complexes with contacts between the RNA minor groove and residues in the N-terminal β strands and between the major groove and residues in the helix−kink−helix motif. We propose that the non-sequence-specific interaction between the zinc fingers of JAZ with dsRNA is dependent only on the overall shape of the A-form RNA.

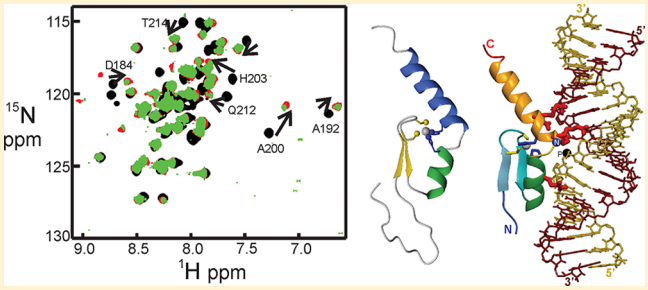

Double-stranded RNAs (dsRNAs) are involved in numerous biological processes, including cellular localization, antiviral responses, RNA interference (RNAi), and viral inhibition of RNAi.[1−9] A specialized class of Cys_2His_2 zinc finger proteins, termed dsRNA-binding zinc finger proteins (dsRBZFPs), bind preferentially to dsRNAs[10−12] and play important roles in the cellular localization of dsRNAs[3] and apoptosis.[13,14] Multiple zinc finger (ZF) domains, each capable of binding to dsRNA, may be present in dsRBZFPs;[3,10,11,13] for example, the dsRNA-binding zinc finger protein a (ZFa) contains seven dsRNA-binding zinc finger domains.[11,15] Just Another Zinc finger protein (JAZ), also known as ZNF346, is a mammalian dsRBZFP with four zinc finger domains, all of which are highly homologous to each other and to the zinc finger domains of *Xenopus laevis* ZFa[3,10,15] (Figure 1A). The mammalian dsRBZFP Wig-1 contains three homologous zinc finger domains and has also been shown to interact with dsRNA. The zinc finger domains of ZFa, JAZ, and Wig-1 are separated by long nonconserved linkers (approximately 20−40 amino acids in length), which are likely to be unstructured.[15]

Published data suggest that all zinc finger domains in these proteins participate in binding to dsRNA[10,12,13] in a sequence-independent fashion.[3,10−12] However, the nature of the RNA targets and the mechanism by which dsRBZFPs recognize dsRNA remains largely unknown, although it has been proposed that the lack of sequence specificity implies that interactions may be determined primarily by the shape of the A-form helix.[12,16] The known binding targets of dsRBZFPs form an evolutionarily disparate but structurally similar group of both endogenous[3] and exogenous[10] double-stranded RNAs. Targets such as the adenoviral VAI RNA[3] contain structural features in addition to canonical A-form double-stranded RNA that could potentially be required to enhance binding, thus providing a measure of specificity. These features include single-strand overhangs at 3′ or 5′ ends, 5′-triphosphate groups (5′-ppp) (which are largely unique to viral RNAs), and internal loops.

To establish whether noncanonical structural features affect the affinity of dsRBZFPs for various RNA targets and to identify a set of minimal RNA and protein constructs for structural studies, we employed electrophoretic mobility-shift assays (EMSA) and NMR spectroscopy to probe the interactions of the JAZ zinc fingers with various dsRNAs. Experiments were also designed to establish whether dsRBZFPs such as JAZ have differential binding activities for host dsRNAs

Received: December 17, 2013
Revised: February 11, 2014
Published: February 13, 2014

   dx.doi.org/10.1021/bi401675h | *Biochemistry* 2014, 53, 1495−1510

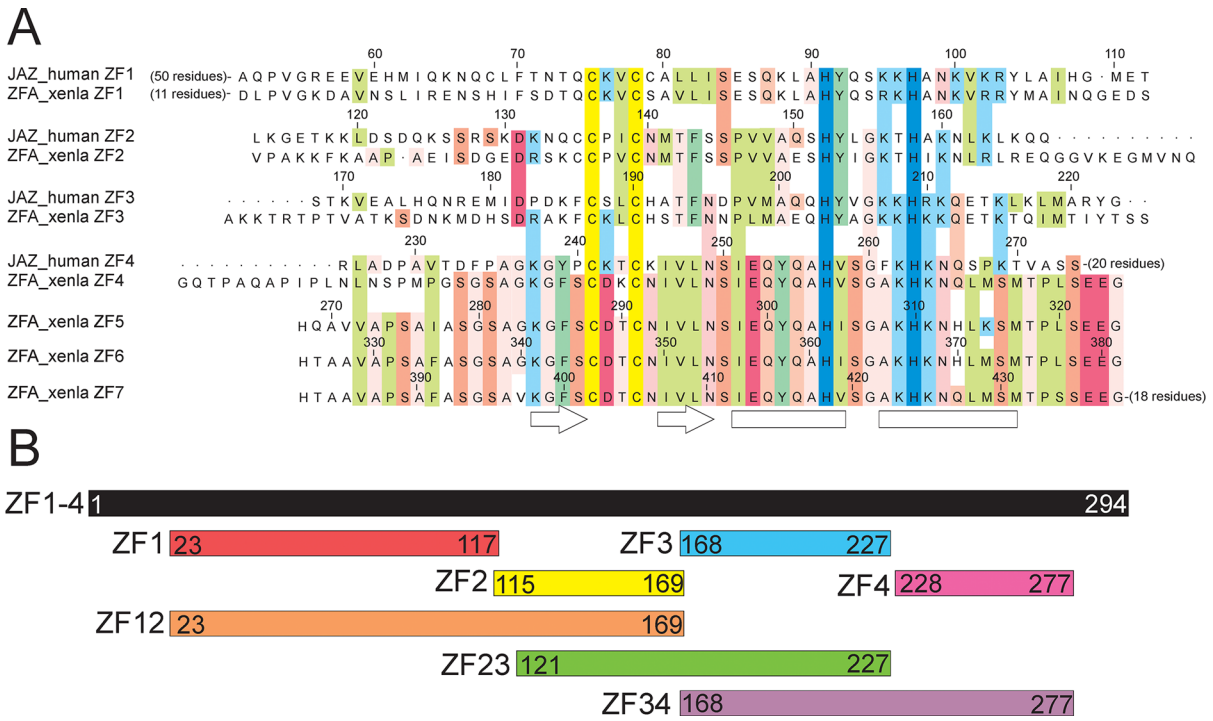

Figure 1. (A) Partial sequence alignment of the zinc finger domains of human JAZ with each other and with those of *Xenopus laevis* ZFa. The sequences are aligned on the highly conserved zinc-binding cysteine and histidine residues in each finger, which are colored yellow and blue, respectively. Sequence identity and similarity between fingers are indicated by colored blocks: green for hydrophobic, blue-green for aromatic, light blue for lysine and arginine, red for aspartate and glutamate, and pink for small and hydrophilic residues. Residue numbers in ZF1−4 correspond to the JAZ sequence, and for ZFa, ZF5−7 correspond to the ZFa sequence. Secondary-structure elements present in the zinc finger domains are indicated at the bottom of the figure (arrow, β-strand; box, α-helix). (B) Schematic representation showing the length of the JAZ zinc finger constructs and the N- and C-terminal residue numbers.

compared to viral RNAs and to evaluate the structural basis for the preference of dsRBZFPs for binding to dsRNA over DNA and tRNA. The contribution of the dsRBZFP linker regions to RNA-binding was also investigated.

Published structures of JAZ zinc finger homologues, including ZF1 and ZF2 from *X. laevis* ZFa[15] and the zinc finger domain from *Saccharomyces cerevisiae* tRNA isopentenyltransferase (IPTase),[17] show a $\beta\beta\alpha\alpha$ fold and helix−kink−helix motif; these structural features appear to be conserved among dsRBZFPs.[18] The specificities of IPTase and JAZ zinc fingers are different: IPTase binds to tRNA,[17] whereas JAZ has very little affinity for tRNA.[10] The structure of the tRNA−IPTase complex reveals that the helix−kink−helix motif contacts the tRNA.[17] The zinc finger domains of JAZ have not been characterized structurally nor are there structures or models of RNA complexes of ZFa or JAZ. In this work, we describe the solution-structure determination of a JAZ zinc finger domain by NMR and structural characterization of the complex between this zinc finger and dsRNA sequences derived from VAI, a viral RNA that is known to bind JAZ, and from pre-miR34a, a human microRNA of known function with long stretches of dsRNA. Although JAZ had not previously been shown to bind to this RNA, it is thought that one of the functions of JAZ may be to interact with pre-miRNAs in the cell,[3] and it was therefore chosen as a likely candidate for *in vitro* testing of JAZ binding to an endogenous RNA. Structural information on nonspecific protein−RNA complexes such as these is limited because of the inherent disorder implied by the absence of specific binding sites on the A-form helix of the RNA. Because the disorder makes solving 3D structures of such complexes by standard NMR or X-ray crystallographic methods challenging, we have employed the high-ambiguity-driven biomolecular docking (HADDOCK) program[19] to obtain 3D models of nonspecific complexes between dsRNA and the JAZ zinc finger domain.

MATERIALS AND METHODS

Protein Construct Design and Sample Preparation. JAZ constructs amplified from a human cDNA library were cloned into pET21a vectors (Novagen). The following recombinant JAZ constructs were expressed: full-length ZF1−4 (residues 1−294), ZF12 (23−169), ZF23 (121−227), ZF34 (168−277), ZF1 (23−117), ZF2 (115−169), ZF3 (168−227), and ZF4 (228−277). Full-length JAZ and the fingers 2 and 3 constructs were prepared as fusions with the B1 domain of protein G (GB1) for EMSA experiments. A JAZ ZF23 (121−227) construct was prepared without a GB1 fusion protein for ITC experiments. All JAZ constructs were expressed in *Escherichia coli* BL21(DE3) DNAY cells cultured in M9 minimal medium to an OD_{600nm} of approximately 0.7−1.0 absorbance units, at which time 1 mM IPTG and 150 μM $ZnSO_4$ (final concentrations) were added to the cultures. Cells were grown at 4 °C for 18 h before harvesting. The pellets were suspended and lysed in 25 mM Tris, pH 7.7, 150 mM NaCl, and 10 mM DTT. Streptomycin precipitation was used for all protein preparations: 2% streptomycin and protease inhibitors without EDTA (Roche) were added to the lysate supernatant with the pH controlled to 8.0. The resultant solution was spun at 5000*g* and then dialyzed into FPLC buffer A (25 mM Tris, pH 7.7, and 2 mM DTT). The supernatants were purified by cation-exchange chromatography using SP Sepharose columns

dx.doi.org/10.1021/bi401675h | *Biochemistry* 2014, 53, 1495−1510

preceded in tandem by HiTrap Q-columns (GE Healthcare). Purification was carried out by FPLC at 4 °C by eluting the SP column with buffer B (25 mM Tris, pH 7.7, and 1 M NaCl). Protein masses were verified using MALDI-TOF MS and SDS PAGE. Highest purity fractions were pooled and exchanged into binding buffer for EMSA experiments. For NMR experiments, SP fractions were pooled and further purified on a Sephadex gel-filtration column (GE Healthcare) (in buffer A) and then exchanged into NMR buffer (30 mM HEPES or 30 mM Tris, pH 7.4, 50 mM KCl, 2 mM DTT, 5 mM $MgCl_2$, 50 μM $ZnSO_4$, and 7% D_2O, degassed and filtered) using a NAP-5 column (GE Healthcare). The protein solutions were then concentrated using centrifugal concentrators. Protein sample concentrations were measured using a Nanodrop spectrophotometer (Thermo Fisher Scientific). No difference in EMSA results was observed using SP fractions compared to fractions from the gel-filtration column.

It is important to note that all work on these proteins was performed in the absence of chelating agents such as EDTA, which are common additives in such experiments but which have deleterious effects on the structural integrity of zinc finger proteins.[20] Indeed, most of the buffers used in our experiments include $ZnSO_4$ to discourage loss of zinc and subsequent unfolding of the proteins.

Nucleic Acid Construct Design and Preparation. All RNA species >44 bp were synthesized by T7 DNA-templated RNA polymerase *in vitro* transcriptions.[21] All VAI RNA constructs >44 bp were cloned into the puC19 vector followed by linearization of the DNA template using restriction enzymes (New England Biolabs) to create T7 templates for transcription reactions. For all oligonucleotides ≤44 bp that were transcribed by T7 reactions, the DNA templates were purchased (IDT). The puC19 plasmid encoding full-length VAI RNA was a gift from Robert J. White, University of Glasgow, Scotland. All RNA oligonucleotides used in EMSA experiments were purified by denaturing gel electrophoresis. The RNA bands were cut out of the gel and then subjected to a crush and soak step (30 mM Tris and 450 mM NaCl, pH 7.8). The RNA was precipitated by diluting the crush and soak solution 10:1 with 99% pure ethanol at −20 °C containing 1 μg/mL of glycogen. Confirmation of RNA purity was established using reverse-phase HPLC and denaturing PAGE. Large-scale T7 DNA-templated RNA polymerase *in vitro* transcriptions (20 mL) were employed to prepare milligram quantities of VAI T57A and T57B RNAs used for NMR titrations; these RNAs were purified by anion-exchange chromatography using HiTrap Q columns (GE Healthcare). The molecular masses of the RNA used for NMR titrations were verified by MALDI-TOF mass spectrometry. DNA was purchased from IDT, and yeast tRNA, from Ambion. The purified nucleic acids were desalted using NAP columns (GE Healthcare) to exchange the buffer into EMSA or NMR buffers without Mg^{2+}. The RNA or DNA oligonucleotides were then heated at 92 °C for 5 min and snap-cooled on ice to produce hairpins (monomolecular structures) or slow-annealed to form duplex RNA. The composition and purity of each annealed product was assessed following phosphorimaging of EMSA gels. After annealing, the nucleic acid solutions (RNA or DNA) used for NMR titrations were further exchanged into NMR buffer and concentrated using a centrifugal concentrator followed by concentration measurements using a Nanodrop spectrophotometer. The pH values of the DNA, RNA, and protein solutions were verified prior to NMR titration experiments.

EMSA Experiments. Protein constructs were exchanged into EMSA binding buffer (30 mM HEPES, pH 7.5, 50 mM KCl, 2 mM DTT, 5 mM $MgCl_2$, 0.1% IGEPAL CA-630, a nonionic detergent (Sigma-Aldrich), and 50 μM $ZnSO_4$) using NAP-5 desalting columns. Binding buffer was used to serially dilute JAZ solutions for equilibration reactions so that each reaction had half of the protein concentration of the preceding sample. Nucleic acid constructs were treated with Antarctic phosphatase (AP) (New England Biolabs) to remove the 5′ phosphate; AP was then inactivated by incubating at 65 °C for 5 min. The nucleic acid solutions were allowed to cool to 25 °C prior to 5′-end ^{32}P-radiolabeling by T4 polynucleotide kinase (New England Biolabs) at 37 °C. The samples were allowed to cool to 25 °C, and the labeled nucleic acids were then purified using Quick-Spin columns (Roche) and heated at 92 °C followed by snap-cooling on ice to anneal to form hairpins or slow annealing to produce oligonucleotide duplexes. Annealed nucleic acids were equilibrated to 25 °C and then added to the binding buffer at a final concentration of 0.5 nM to create master mix solutions (MM). The RNase inhibitor RNasin (Promega) and nonspecific competitors (50 nM cold tRNA [unless otherwise stated] and 25 nM bovine serum albumin) were added to the MM. Assays were performed by adding 16 μL of MM to JAZ solutions for a final volume of 20 μL each. Samples were equilibrated at 25 °C for 1 h prior to electrophoresis on a 7% native polyacrylamide Tris-borate gel free of EDTA. To each sample was added 4 μL of loading buffer (5% Ficoll, 0.02% xylene cyanol, and 20% glycerol). Gels were run at 4 °C and 600 V for 45 min and then dried and exposed to a phosphor-intensifier screen (Molecular Dynamics). Gels were scanned using a Storm-840 Imager (Molecular Dynamics).

Because multimeric binding was observed for most complexes, affinities could not be measured by quantitative fitting of the binding data; relative affinities (C_{50}) were estimated from the concentration of JAZ at which half of the RNA probe was bound.

Isothermal Titration Calorimetry. ITC experiments of JAZ ZF1 were performed at 25 °C using an Omega VP-ITC instrument (MicroCal). Samples were exchanged into ITC binding buffer using NAP-25 desalting columns. The ITC binding buffer was 50 mM Tris-HCl, pH 7.4, 50 mM KCl, 5 mM $MgCl_2$, 1 mM TCEP, and 50 μM $ZnSO_4$ (50 mM HEPES, pH 7.3, 50 mM KCl, 50 μM $ZnSO_4$, 5 mM $MgCl_2$, and 1 mM TCEP for the JAZ ZF23 ITC experiments). The protein and RNA solutions were repeatedly exchanged into ITC buffer and concentrated using centrifugal concentrators. The pH values of the DNA, RNA, and protein solutions were verified prior to ITC experiments. Protein and RNA concentrations were measured by absorbance values at 280 and 260 nm, respectively, using a Nanodrop spectrophotometer. JAZ ZF1 (syringe) at 230 μM was titrated into 23 μM VAImin RNA (cell). For the ITC experiments of JAZ ZF23, RNA (syringe) at 300−580 μM was titrated into 18−30 μM JAZ ZF23 (cell). Each ITC experiment was started by a single injection of 5 μL followed by 29 injections of 10 μL until all of the solution (RNA or protein) in the syringe was injected into the cell. Final molar ratios of up to 2.8:1 for the JAZ ZF1/RNA and up to 6.1:1 JAZ ZF23/RNA were obtained. The heats of dilution were small and subtracted from the calorimetric data. Thermodynamic parameters of the binding isotherm were fitted to a one-site binding model using Origin 7 software (MicroCal). Duplicate experiments were obtained for JAZ ZF1,

and for JAZ ZF23, four experiments were obtained (two experiments per RNA).

Binding Affinities from Chemical-Shift Perturbations. Dissociation constants of JAZ ZF2 and JAZ ZF3 with VAImin RNA were calculated from the changes in the chemical shifts observed in $^{1}H-^{15}N$ HSQC spectra in quantitative NMR titrations using a two-site binding model as previously described.[48] The binding affinities for the primary and secondary binding sites were calculated by globally fitting the chemical shift changes of the protein backbone resonances (both ^{1}H and ^{15}N) as a function of the molar ratio of RNA-to-protein. The ^{1}H and ^{15}N titration data were fitted using the program *nmrKd2* (developed by Dr. M. Arai). The titration data of JAZ ZF2 were initially fitted to a one-site model, and the K_d value obtained from this initial fit was used to approximate the dissociation constant of the primary binding site (K_{d1}); the program was then used to fit the data to a two-site binding model to calculate the dissociation constant of the secondary binding site (K_{d2}). Because of the greater uncertainty in the measurement of the protein concentration compared to that of RNA, the concentrations of JAZ ZF2 and JAZ ZF3 were allowed to vary during fitting of the experimental data; this is the most accurate procedure for calculating K_d values from these experiments.[22] The graphs of $\Delta\delta$ plotted as function of molar ratio have corrected protein concentrations as calculated by the global fitting parameters.[23]

NMR Experiments and Structure Calculations. NMR spectra were acquired on Bruker DRX600, DMX750, and AVANCE800 spectrometers at 298 K. NMR data were analyzed using XWINNMR (Bruker), TopSpin (Bruker), NMRpipe,[24] and NMRview.[25] Backbone-resonance assignments for single zinc finger protein constructs were made using standard HNCO, HNCA, HNCOCA, HNCACB, and CBCACOHN spectra.[26,27] The concentrations of JAZ NMR samples were 50−450 μM. The NMR buffer was 30 mM HEPES or 30 mM Tris, pH 7.4, 50 mM KCl, 2 mM DTT, 5 mM $MgCl_2$, 50 μM $ZnSO_4$, and 7% D_2O. Resonance assignments were deposited in the Biological Magnetic Resonance Bank (accession numbers 17630(ZF1), 17631-(ZF2), 17679(ZF3), and 17672(ZF4).

Side-chain resonances for JAZ ZF3 were assigned from ^{15}N-NOESY-HSQC, ^{15}N-TOCSY-HSQC, ^{13}C-NOESY-HSQC, HCCH-TOCSY, and HCCH−COSY spectra.[28] Structures of JAZ ZF3 were calculated using manually assigned unambiguous distance restraints from ^{15}N-NOESY-HSQC and ^{13}C-NOESY-HSQC spectra, ϕ and ψ torsion angles derived from chemical shifts using TALOS+,[29] and zinc coordination geometry restraints as described previously.[15] Initial structures were calculated using CYANA.[30] The final set of distance and angle constraints was used to produce 500 structures in CYANA, and the 100 structures with the smallest constraint violations were refined by molecular dynamics using AMBER 9.[31] The final refinement was performed by simulated annealing and energy minimization that employed a generalized-Born (GB) continuum solvent model.[32] PROCHECK was used for analysis of the JAZ ZF3 NMR structural ensemble.[33] The NMR structures of the free form of JAZ ZF3 were deposited in the protein data bank (PDB) under accession number 2MKD.

HADDOCK Modeling. Models of the complexes formed by interaction of JAZ ZF2 (homology modeled using the Phyre webserver[34]), JAZ ZF3, and ZFa ZF1[15] with a minimal binding sequence of A-form dsRNA (determined during the NMR experiments to be 19 base pairs) were generated using HADDOCK version 1.2.[19] The complex between JAZ ZF3 and dsRNA was typical and is described in detail. Protein and nucleic acid were docked as rigid bodies using ambiguous interaction restraints with energy minimization. The best scoring complexes (based on the HADDOCK score values) were then transferred to semiflexible refinement stage. Again, best scoring complexes were then moved to the final structural refinement step employing an explicit solvent model (H_2O).[19] The expert interface of the HADDOCK webserver was used for modeling. This interface of the HADDOCK webserver allows for residue- and nucleotide-level docking parameters for proteins and RNA (or DNA) as well as custom distance constraints. Distance restraints to the Zn ligands were added to preserve the correct geometry of the Zn coordination. HADDOCK complexes were produced using surface-exposed residues with weighted ^{1}H and ^{15}N chemical-shift $\Delta\delta$ (ppm) values $\geq$ 0.9 times the standard deviation of all measurable chemical-shift perturbation data for the residue-level (ambiguous interaction restraints) as docking restraints to the idealized A-form model of VAIminMut RNA, which contains only canonical Watson−Crick base pairs. Chemical-shift perturbations were calculated using the equation

$$\Delta\delta\mathrm{av} = \sqrt{(\Delta\delta HN)^2 + \left(\frac{\Delta\delta N}{5}\right)^2}$$

The idealized A-form VAIminMut RNA duplex (19 base pairs) was created using the make-NA webserver (http://structure.usc.edu/make-na/).[35] For all docking procedures, ambiguous RNA-docking restraints were used for all nucleotides (except for the terminal nucleotides), which allow RNA-contacting residues of the zinc fingers (ambiguous interaction restraints) to interact with any set of ≤17 bp of the duplexes. Ambiguous interaction restraints to nucleotides 3−17 (strand 1) and nucleotides 22−36 (strand 2) were applied. Some residues in JAZ ZF3 that exhibited substantial chemical-shift changes ($\Delta\delta$) upon addition of RNA are buried within the zinc finger domain (i.e., are not surface-exposed) and therefore are predicted not to contact the RNA directly. These residues were not utilized as ambiguous interaction restraints for the HADDOCK modeling because their backbone resonances are likely perturbed indirectly by local changes in the protein structure upon binding RNA. The HADDOCK program was allowed to define passive residues (residues near the interface that may play a role in the formation of the complex) as docking parameters automatically. Distance restraints were used to preserve the Zn coordination in all zinc finger domains. Those structures with the highest HADDOCK scores were designated as the best models. The residues defined as ambiguous interaction restraints for the JAZ ZF3−RNA complex are active residues 191, 195, 198, 203, 206, 207, 208, 209, 211, and 214. The model with the highest HADDOCK score was deposited in the PDB under accession number 2MKN.

RESULTS

Design of Protein and RNA Constructs. The JAZ protein constructs, shown schematically in Figure 1B, include four small proteins representing the individual zinc fingers, 3 two-finger constructs (ZF12, ZF23, and ZF34), and the full-length zinc finger domain (ZF1−4). The constructs containing the first zinc finger (ZF1, 95 residues, and ZF12, 147 residues) are longer than the other one- and two-finger constructs (55, 60, and 49 residues for ZF2, ZF3, and ZF4, respectively, and 107

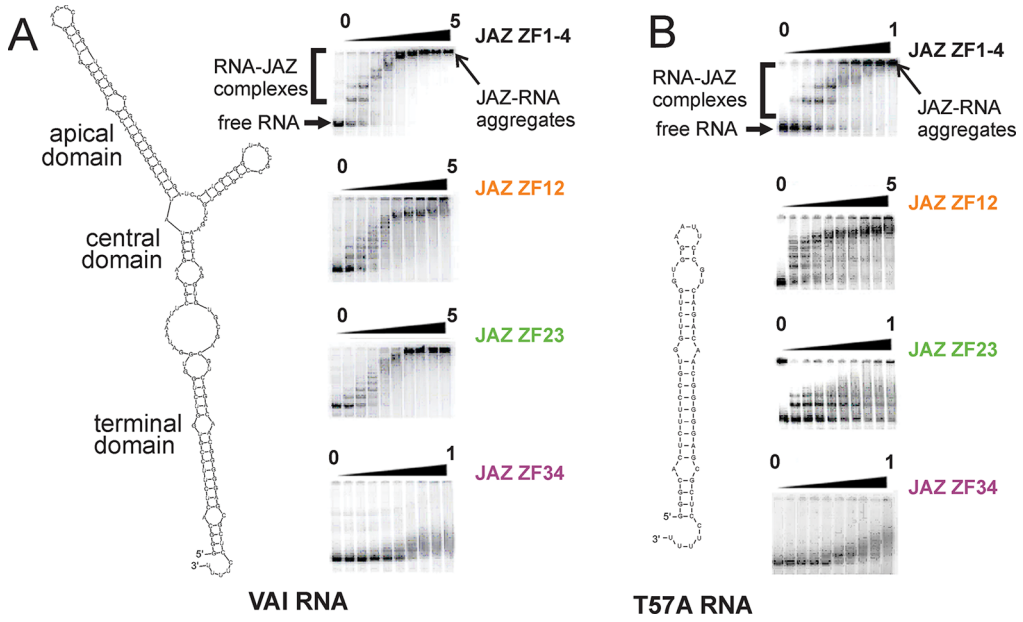

Figure 2. (A) EMSA gels showing binding of full-length (ZF1−4) and two-finger (ZF12, ZF23, and ZF34) JAZ constructs to full-length VAI RNA. In each gel, the first lane is free RNA. In the second lane, the protein concentration is 20 nM (4 nM for ZF34). In each subsequent lane, the protein concentration is doubled until [JAZ] = 5 μM (1 μM for ZF34) in the tenth lane. (B) EMSA gels showing binding of JAZ ZF1−4, ZF12, ZF23, and ZF34 to T57A RNA. In each gel, the first lane is free RNA. In the second lane, the protein concentration is 20 nM (4 nM for ZF34 and ZF23). In each subsequent lane, the protein concentration is doubled until [JAZ] = 5 μM (1 μM for ZF34 and ZF23) in the tenth lane. The figures of the RNA structures were produced using Mfold.[38] Full sequences with RNA bases shown in larger type are given in Supporting Information Figures S2 and S3. The JAZ constructs are identified with colors corresponding to those in Figure 1B.

Table 1. Estimates of Relative Affinity of RNAs for JAZ Zinc Fingers

		no. base pairs[48]					binding to JAZ	
RNA	no. nucleotides	W−C	wobble	no. bulge	no. loop	no. overhang	EMSA (ZF34)[a]	NMR (ZF3)[a]
VAI								
full-length	160	46	8	16	31	5 (CUUUU)	++	nd
apical	50	20	1	3	5 (AAUU)	0	++	++
T52	52	17	3	8	4 (AAUU)	0	++	nd
T57A	57	17	3	8	4 (AAUU)	5 (CUUUU)	++	++
T57B	57	17	3	8	4 (GGGA)	5 (CUUUU)	++	++
T57C	57	18	3	6	4 (AAUU)	5 (CUUUU)	++	nd
T57D	57	18	3	6	4 (AAUU)	5 (CUUUU)	++	nd
T57E	57	20	2	6	4 (AAUU)	5 (CAAAA)	++	nd
T84	84	21	4	12	17 (GGGA)	5 (CUUUU)	++	nd
T44	44	13	3	4	3	5 (CUUUU)	+	nd
T37	37	10	3	4	4	5 (CUUUU)	+	++
duplex I	53	17	3	8	0	5 (CUUUU)	+	nd
duplex II	49	17	3	4	0	5 (CUUUU)	+	nd
duplex III	61	21	3	8	0	5 (CUUUU)	+	++
duplex IIIA	66	21	3	8	0	10 (2× CUUUU)	+	nd
T57 DNA	57	17	3	8	4 (AATT)	5 (CAAAA)	−	−
VAImin	38	16	2	2	0	0	nd	++
VAIminMut	38	19	0	0	0	0	nd	++
ssRNA	10	0	0	0	0	0	−	nd
pre-miR34a		33	7	16	13	1	++	nd

[a]++ corresponds to affinity (C_{50}) ~ 0.05−0.2 μM, +, to C_{50} ~ 0.2−2 μM, and −, to C_{50} > 2 μM.

and 110 residues for ZF23 and ZF34, respectively). The extended N-terminal sequence of the ZF1 and ZF12 constructs was necessary for protein expression, as shorter constructs were not well-expressed.

Two RNAs were used to characterize the binding specificity of the JAZ zinc fingers: adenoviral VAI RNA[36] and human pre-miR34a.[37] Both RNAs contain substantial stretches of base-paired double-strand duplex, identified by Mfold,[38] with loops and bulges in a number of locations. An important difference between VAI and pre-miR34a is the presence of a five-nucleotide overhang at the 3′ end of VAI.

Constructs of VAI were designed on the basis of the sequence of the apical and terminal domains (identified in Figures 2A, S2, and S3). The terminal domain was chosen for

dx.doi.org/10.1021/bi401675h | Biochemistry 2014, 53, 1495−1510

an extensive study of the dependence of the affinity of JAZ upon length and local structure of the RNA with the most frequently used fragment, T57, containing 57 nucleotides from the terminal domain connected by tetraloop sequences of high stability. Oligonucleotide T57A has the tetraloop sequence A−A−U−U, whereas T57B has the loop sequence G−G−G−A.[39] The roles of specific features of the VAI Mfold model, such as the 3′ overhang and the various non-Watson−Crick base pairs and bulges, were evaluated using variant nucleotide sequences, generally by substitution with canonical G−C base pairs. Control experiments included tests of the affinity of the JAZ fingers for a DNA duplex of sequence corresponding to that of T57A RNA and for a short single-stranded RNA. Following an extensive series of EMSA and NMR experiments to establish the minimal dsRNA constructs that would support binding of a single zinc finger, a duplex termed VAImin was designed and utilized for quantitative estimations of the affinities of the various JAZ zinc finger constructs.

Affinity of JAZ Zinc Fingers for dsRNA. Adenoviral VAI RNA binds tightly to JAZ[3] and provides a structural template for the investigation of the mechanisms by which JAZ recognizes dsRNA. EMSA experiments were used to probe the RNA interactions of full-length JAZ ZF1−4 and the 3 two-finger constructs, ZF12, ZF23, and ZF34. Figure 2A shows that each of these proteins binds to full-length VAI RNA. Figure 2A also shows that multimeric JAZ−RNA complexes are formed at higher protein concentrations, likely because of binding of multiple copies of the protein to the RNA; the formation of multimeric species precludes quantitative analysis of the binding curves to give accurate dissociation constants. The EMSA results were analyzed qualitatively by estimating the concentration of JAZ at which half of the ^{32}P-labeled RNA probe was bound (C_{50}). JAZ ZF1−4 has the highest apparent affinity for full-length VAI RNA ($C_{50} \approx 20$ nM); the two-finger constructs JAZ ZF12 and JAZ ZF23 have a reduced affinity ($C_{50} \approx 40$ nM), and JAZ ZF34 has the lowest affinity ($C_{50} \approx 60$ nM). The JAZ ZF34−RNA complexes showed diffuse gel shifts and smearing of the labeled RNA probe at higher protein concentrations, probably because of the dissociation of the complex during the running of the gel.

To determine the minimal length of RNA that would bind the JAZ zinc fingers, a number of smaller fragments of the VAI RNA were used as probes in EMSA experiments. An example of the behavior of one of these fragments, T57A, which binds the JAZ zinc finger constructs with affinities comparable to those of the full-length RNA, is shown in Figure 2B. Similar to their behavior with full-length VAI, JAZ ZF1−4, ZF12, and ZF23 all bind to T57A RNA with high affinity and in a multimeric fashion. Below a certain threshold length, the affinity was significantly lowered. Estimates of the relative affinities of the JAZ fingers for representative dsRNAs of various lengths and compositions are shown in Table 1. Images of EMSA gels corresponding to representative experiments summarized in this figure are shown in Figure S1, and a full compendium of all of the RNAs studied in this work is given in Figures S2 and S3.

Variants of the terminal domain of VAI were used to test the effect of the presence of overhangs and irregular elements on JAZ binding affinity. Binding assays tested whether JAZ binding was influenced by structural features such as loops, bulges, and unpaired bases, which perturb the A-form RNA structure typical of hydrogen-bonded Watson−Crick base pairs. The comparisons were made using JAZ ZF34, which binds to T57A RNA with a lower apparent affinity than the other JAZ constructs (Figure 2B) but for which the multimeric complexes are less evident. In addition, the tighter-binding JAZ constructs frequently created well-shifts (all the labeled RNA probe was shifted by the protein, but the complexes could not enter the gel even at low protein concentrations). The affinity of JAZ ZF34 for the T52 VAI RNA, where the 3′ overhang (5′-CUUUU-3′) present in T57A is absent (Figure S1A), is similar to that of T57A (Figure 2B), suggesting that a 3′ overhang is not necessary for binding. The influence of non-Watson−Crick base pairs (G−A, A−C, and G−U) in the T57A sequence on the affinity of JAZ ZF34 was tested by examining the behavior of variants where these noncanonical base pairs were substituted by Watson−Crick pairs, generally G−C. Table 1 shows that the effects of these variant RNA sequences (shown in Figure S2) are negligible: all of the hairpin RNAs have affinities for JAZ ZF34 similar to that of T57A RNA ($C_{50} \approx$ 60−80 nM). The apical domain construct of the VAI Mfold model (VAI Apical) contains slightly different features, including an A−C base pair and a bulge that arises because of an unpaired guanine. This RNA hairpin has a pentaloop instead of the tetraloops of the VAI terminal-domain hairpin constructs. EMSA experiments show that JAZ ZF34 binds to VAI Apical with a slightly weaker apparent affinity ($C_{50} \approx 120$ nM) compared to the terminal RNA hairpin constructs, possibly indicating a slight effect on the affinity of an unpaired bulge. Altogether, the EMSA binding data for the hairpin dsRNA species indicate that when the A-form helix is perturbed in a manner that preserves base pairing, even if that pairing is noncanonical, the affinity for JAZ ZF34 is not significantly affected. However, a structural perturbation that disrupts base pairing in the context of an otherwise duplex RNA may have a small effect on binding affinity. These binding studies suggest that JAZ ZF34 recognizes extended A-form helices independent of either sequence or the presence of local noncanonical structures.

More significant structural perturbations of canonical A-form RNA are found in the central domain of the VAI Mfold model. The effect of the internal loop in VAI RNA on JAZ ZF34 binding was tested with the T84 RNA construct (Figure S2). Once again, EMSA assays show that JAZ ZF34 binds T84 RNA with apparent affinity ($C_{50} \approx 60$ nM) similar to those of the T57 RNAs, suggesting that large internal loops do not contribute to JAZ−RNA interactions.

Somewhat surprisingly, the affinity of JAZ ZF34 for duplex (nonhairpin) RNA with the same sequence as that of T57 (duplex I) appears to be weaker ($C_{50} \approx$ 500−1000 nM) than that of the hairpin RNA (Figure S1C). Nevertheless, RNA variants designed to test the effects of non-A-form structures, helix-perturbing structural elements, and extensions of stable base-paired sequences at either end on recognition by JAZ ZF34 show similar affinities to duplex I ($C_{50} \approx 500$ nM). Additionally, JAZ ZF34 binds to a dsRNA with two 3′ overhangs, (duplex III 2 × 3′) with similar affinity, confirming the results with hairpin T52 that suggest that 3′ overhangs do not influence JAZ−RNA interactions. Although the apparent affinity of JAZ ZF34 for duplex RNA is reduced compared to that for hairpin RNA of the corresponding sequence when measured by EMSA, these RNA constructs bind with comparable affinity when measured by NMR (see later section). Because the presence or absence of a hairpin loop sequence is unlikely to influence affinity in a sequence-specific manner, we suggest that the lower affinity of the duplex RNAs

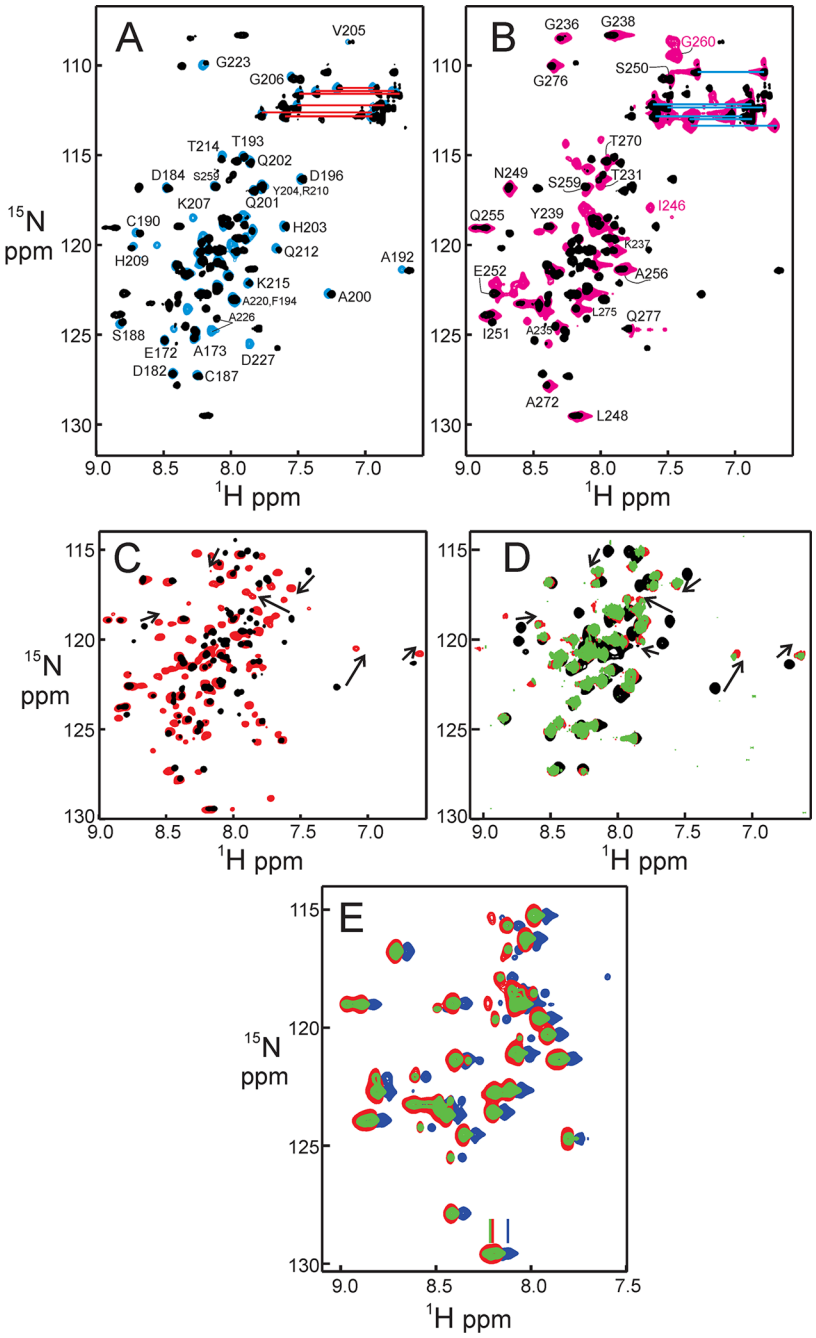

Figure 3. ^{1}H−^{15}N HSQC spectra of JAZ zinc finger domains. (A) Superposition of the 600 MHz spectrum (298 K) of ZF34 (black) with that of ZF3 (blue). Red horizontal lines denote resonances of side-chain carboxamide groups of Asn and Gln residues. Representative assignments are indicated. (B) Superposition of the 600 MHz spectrum (298 K) of ZF34 (black) with that of ZF4 (magenta). Blue horizontal lines denote resonances of side-chain carboxamide groups of Asn and Gln residues. Representative assignments are indicated. Labels in red indicate resonances that are observed for ZF4 but not for ZF34. (C) Superposition of part of the 800 MHz spectrum (298 K) of 100 μM ZF34 (black) with that of 100 μM ZF34 in the presence of 220 μM VAI T57A RNA (red). Some weak peaks are missing in the spectrum of ZF34 because of exchange broadening. (D) Superposition of part of the 600 MHz spectrum (298 K) of 50 μM ZF3 (black) with that of 63 μM ZF3 in the presence of 120 μM VAI T57B (red) and that of 50 μM JAZ ZF3 in the presence of 100 μM duplex III (green). (E) Superposition of part of the 750 MHz spectrum (298 K) of 100 μM ZF4 (blue), that of 100 μM ZF4 in the presence of 200 μM duplex III RNA (red), and 100 μM ZF4 in the presence of 300 μM duplex III RNA (green). The blue (free protein) spectrum has been offset to the right for clarity by an amount indicated by the vertical lines at the bottom of the figure.

observed by EMSA is likely due to lowered stability or increased off-rate of the duplex RNA from the complex under the conditions of the EMSA experiment; the engineered tetraloops clearly stabilize the dsRNA helical structure in the hairpins. This subtle discrimination of hairpins over duplexes by JAZ ZF34 suggests that dsRNA stability influences JAZ−RNA interactions, but our results nevertheless confirm that JAZ ZF34 is capable of binding to both duplex and hairpin RNAs.

EMSA experiments confirm that JAZ ZF34 does not interact with single-stranded RNA (ssRNA) (Figure S1D). That the interactions observed in the EMSA experiments truly represent the formation of protein−RNA complexes is shown by the

dx.doi.org/10.1021/bi401675h | *Biochemistry* 2014, 53, 1495−1510

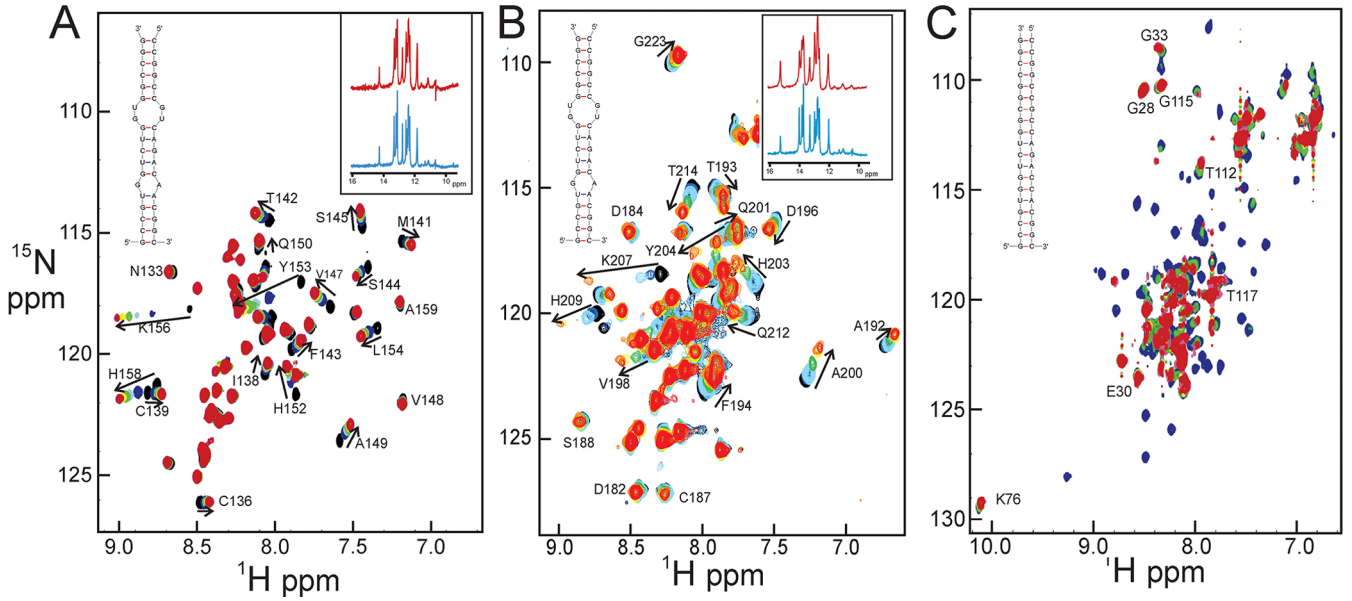

Figure 4. (A) NMR titration of JAZ ZF2 with increasing concentrations of VAImin RNA. The spectra are colored by molar ratio: free ZF2, black and [RNA]/[ZF2] 0.5, blue; 1.0, cyan; 1.5, green; 2.2, yellow; 3.7, magenta; and 3.8, red. Inset: 1D ^{1}H spectra (imino proton region) of free VAImin RNA (cyan) and of a 1:1 complex with JAZ ZF2 (red). The structure of VAImin is shown at the top left. (B) NMR titration of JAZ ZF3 with increasing concentrations of VAImin RNA. The spectra are colored by molar ratio: free ZF3, black and [RNA]/[ZF3] 0.2, blue; 0.4, cyan; 0.6, green; 0.8, yellow; 1.0, orange; and 2.0, red. Inset: 1D ^{1}H spectra of free VAImin RNA (cyan) and of a 1:1 complex with JAZ ZF3 (red). The structure of VAImin is shown at the top left. (C) NMR titration of JAZ ZF1 with VAIminMut RNA. The spectra are colored by molar ratio: free ZF1, blue and [RNA]/[ZF1] 0.04, cyan; 0.1, green; 0.2, yellow; 2.0, magenta; and 2.5, red. The structure of VAIminMut is shown at the top left.

displacement of the ^{32}P-labeled RNA by excess cold RNA (Figure S1E). A similar experiment evaluating competition by excess tRNA showed that the JAZ proteins preferentially bind dsRNA rather than tRNA (Figure S1F).

Our EMSA results confirm that JAZ ZF34 is a nonspecific dsRNA-binding protein. The length of the A-form helix may therefore be the main determinant for the formation of JAZ–RNA complexes. RNA constructs of various lengths based on the terminal domain of the VAI Mfold model were tested by EMSA to determine the length of dsRNA helices necessary for high-affinity interactions with JAZ. A significantly lower affinity of JAZ ZF34 is observed for the shorter terminal domain hairpins T37 (total length 14 base pairs, consisting of 10 Watson–Crick base pairs, three G–U wobble pairs, and one non-hydrogen-bonded C–A pair) and T44 (total length 17 pairs, consisting of 12 Watson–Crick base pairs, three G–U wobble pairs, and two non-hydrogen-bonded pairs) ($C_{50} \approx 500$ nM) compared to T57A (total length 24 pairs, consisting of 17 Watson–Crick base pairs, five G–U wobble pairs, and two non-hydrogen-bonded pairs) ($C_{50} \approx 60$ nM), suggesting that the minimal RNA-binding site for JAZ ZF34 is between 16 and 22 base pairs.

Interactions between JAZ and endogenous dsRNA have not previously been reported. The endogenous human microRNA pre-miR34a was tested by EMSA for binding to JAZ ZF34 and JAZ ZF23. The apparent binding affinities were similar to the corresponding affinities for the binding of the two proteins to the VAI T57A RNA ($C_{50} \approx 80$ nM for ZF34 and ≈ 40 nM for ZF23). These results demonstrate that JAZ ZF34 and ZF23 can interact with both endogenous and exogenous dsRNAs with comparable affinities, suggesting that JAZ is unable to differentiate between host dsRNAs and viral RNAs.

NMR Characterization of the Interaction of JAZ ZF3 and ZF4 with dsRNA. Because JAZ ZF34 appeared to have the least complicated interaction with dsRNA from the EMSA experiments and because this protein had been used most extensively in the EMSA characterization of the RNA binding, we chose to examine its RNA interactions by NMR, using JAZ ZF34 and its single zinc finger daughter constructs JAZ ZF3 and ZF4. The ^{1}H–^{15}N HSQC spectra of the three ^{15}N-labeled proteins are well-resolved, and the cross peaks in the spectrum of each individual finger overlay well with a subset of the cross peaks in the ZF34 spectrum, indicating that the zinc finger domains are independently folded and largely monomeric in solution (Figure 3A,B). Size-exclusion chromatography also indicated that the proteins were monomeric under all solution conditions studied. Titrations of VAI T57A RNA into ^{15}N-labeled JAZ ZF34 show shifts of the amide cross peaks in the ^{1}H–^{15}N HSQC spectrum of the protein upon addition of RNA (Figure 3C), indicating the formation of a protein–RNA complex consistent with the EMSA results shown in Figure 2B. One-dimensional ^{1}H NMR spectra of the T57A RNA show that the resonances of the hydrogen-bonded imino protons are slightly broadened by the addition of ZF34 but are not significantly shifted, an indication that the RNA remains in A-form conformation upon binding to JAZ (Figure S4). A similar result was obtained when duplex III was added to ZF34 (Figure 3D). The shifted cross peaks in Figure 3C,D correspond almost entirely to those of ZF3, a result that is corroborated by the observation of similar shifts upon addition of RNA to the single zinc finger protein ZF3. Moreover, the spectrum of the single zinc finger ZF4 is unperturbed by the addition of RNA (Figure 3E). The NMR results show that JAZ ZF3 binds to dsRNA in a similar manner whether it is a single finger or part of a two-finger construct and that it binds with similar affinity to hairpin or nonhairpin RNA. The binding observed to duplex III RNA suggests that tetraloops are not specifically recognized by JAZ ZF3 and thus, as suggested previously, that the increased

dx.doi.org/10.1021/bi401675h | *Biochemistry* 2014, 53, 1495–1510

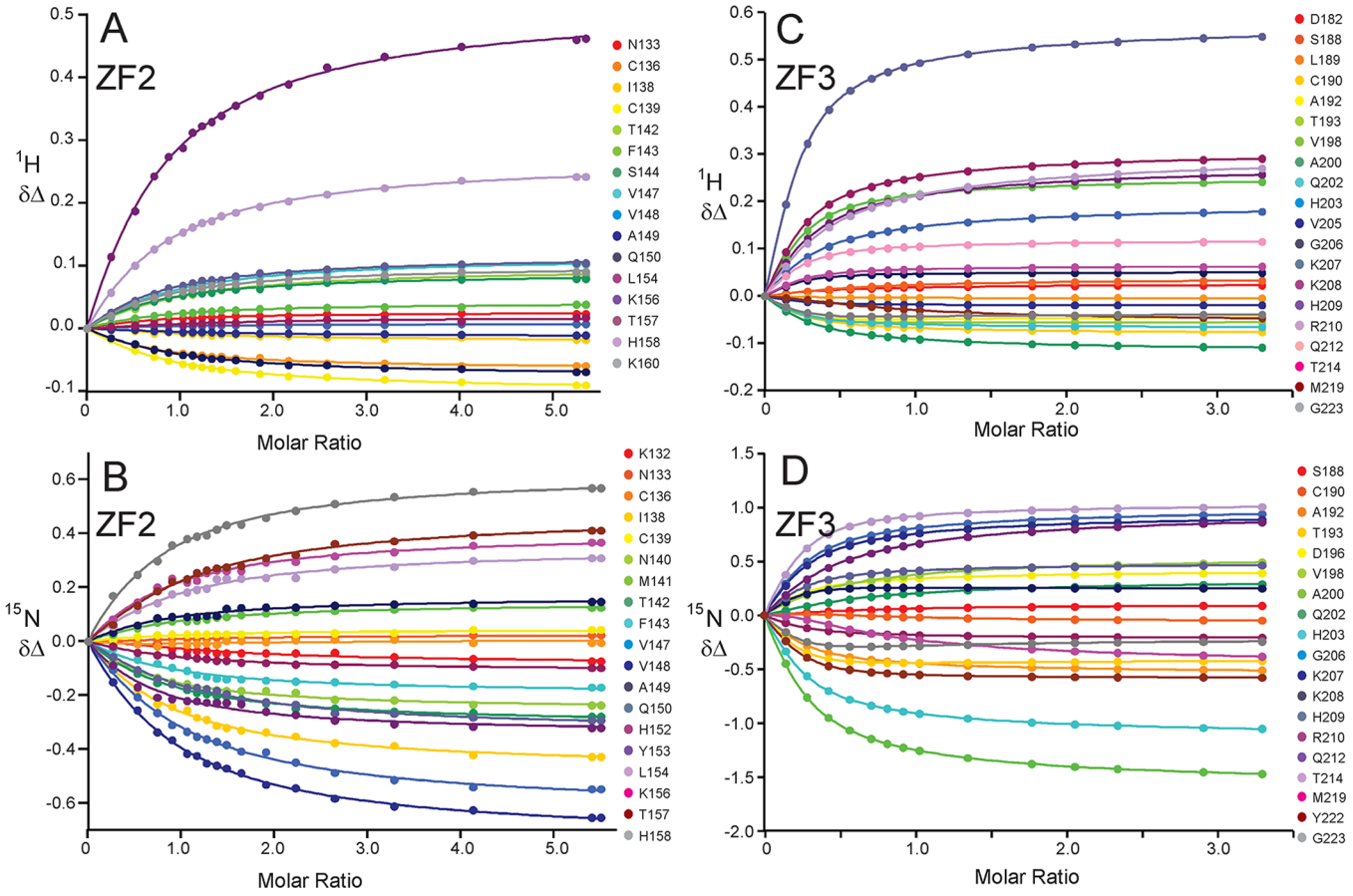

Figure 5. Chemical-shift perturbations for all measurable amide resonances upon binding VAImin RNA (derived from the data of Figure 3) plotted as a function of the molar ratio of [RNA]/[ZF]. Experimental data are represented by filled circles; lines of corresponding colors show the results obtained from global fits of all of the ^{1}H and ^{15}N $\Delta\delta$ data for a given titration to a two-site binding model using the program *nmrKd2*.[23] (A) ^{1}H data for the ZF2/VAImin RNA titration. (B) ^{15}N data for the ZF2/VAImin titration. (C) ^{1}H data for the ZF3/VAImin titration. (D) ^{15}N data for the ZF3/VAImin titration.

apparent affinity for hairpin RNAs compared to the equivalent duplex sequence in EMSA experiments is most likely due to an increase in the stability of the free RNA hairpin compared to the duplex. These results further indicate that JAZ ZF3 is solely responsible for the RNA interaction of JAZ ZF34, which is consistent with the lower apparent affinity of JAZ ZF34 for dsRNA compared with those of the other two-finger protein constructs.

NMR experiments were used to identify minimal RNA constructs capable of binding to single JAZ zinc finger domains through observation of appreciable changes in the chemical shifts of the JAZ zinc fingers in the presence of excess RNA. Appreciable binding to JAZ ZF3 was observed for full-length VAI, the VAI apical domain, and the shorter VAI terminal domain constructs T57A and T52. Both NMR and EMSA data indicate that the T37 dsRNA (total length 14 pairs, with 10 Watson−Crick base pairs, three G−U wobble pairs, and one non-hydrogen-bonded C−A pair in the Mfold model) is too short for binding to JAZ fingers. A minimal RNA duplex VAImin (total length 19 pairs, consisting of 16 Watson−Crick base pairs, two G−U wobble pairs, and one non-hydrogen-bonded G−A pair in the Mfold model) was designed on the basis of the terminal domain of VAI. Because the spectra of JAZ ZF3 in complex with VAImin and with T57B RNA are similar, the bound form of JAZ ZF3 must be structurally similar in the two complexes and we therefore propose that A-form RNAs approximately 19 base pairs in length are sufficient for binding to JAZ ZF3.

The HSQC spectra of ZF3 bound to VAImin and to a variant RNA, VAIminMut, where all of the noncanonical base pairs are mutated to G−C base pairs are almost identical (Figure S4A). This observation supports the EMSA results that show that JAZ−RNA interactions are not influenced by tetraloops, overhanging nucleotides, or non-Watson−Crick base pairs and their associated structural perturbations of the A-form helix. The NMR titration results also show that the presence or absence of 5′-triphosphate groups does not affect the binding of JAZ. JAZ ZF3 can bind to dsRNAs that possess 5′-ppp groups, such as VAI T57B (prepared by transcription reactions), and also to RNAs lacking the 5′-ppp groups, such as the VAImin RNA (prepared by chemical synthesis).

Consistent with published observations,[10] NMR titration data indicate JAZ ZF3 binds only weakly to a DNA duplex with sequence corresponding to the VAImin RNA sequence (Figure S4B): only very small chemical-shift perturbations of a few of the protein-backbone resonances are observed. Most JAZ ZF3 backbone amide resonances are unchanged even in the presence of excess VAImin DNA. The imino proton resonances of the DNA indicate that the DNA remains in duplex form in the presence of JAZ ZF3. The binding affinity of JAZ ZF3 to VAImin DNA is too weak to quantitate using NMR, EMSA, or ITC methods.

dx.doi.org/10.1021/bi401675h | *Biochemistry* 2014, 53, 1495−1510

Quantitative Estimates of JAZ–RNA Binding by NMR. NMR titration experiments were employed to measure the binding affinities of JAZ ZF2 and JAZ ZF3 for VAImin RNA by quantitation of chemical-shift changes of the protein-backbone resonances in $^{1}H-^{15}N$ HSQC spectra of JAZ ZF2 (Figure 4A) and JAZ ZF3 (Figure 4B) as increasing amounts of VAImin RNA were added. Shifted cross peaks are broadened in some cases because of the on–off exchange rates of the complexes. Broadening is more pronounced for ZF3, an indication that the ZF3–VAImin RNA complex has a slightly higher affinity (slower off-rate) than the ZF2–VAImin complex. For ZF1 (Figure 4C), the resonances are broadened by the same mechanism to such an extent that the NMR data cannot be used to obtain binding constants.

The NMR titration data for both ZF2 and ZF3 indicate that VAImin RNA binds two zinc finger domains at saturation through a primary binding site with a relatively high affinity and a secondary binding site with a lower affinity. Binding affinities were determined by globally fitting the chemical-shift changes of the protein-backbone resonances (both ^{1}H and ^{15}N) as a function of the molar ratio of RNA-to-protein for each titration point using a two-site binding model[22] with the program *nmrKd2*.[23] Results are shown in Figure 5. For the JAZ ZF3–VAImin RNA complex, the NMR data were fit to give K_{d1} = 8 ± 1 μM and K_{d2} = 121 ± 10 μM. For JAZ ZF2, the dissociation constants for VAImin RNA were estimated to be K_{d1} = 10 μM (fixed during fitting) and K_{d2} = 92 ± 9 μM.

Dissociation constants for the JAZ ZF1–VAImin RNA complex could not be determined using NMR titration experiments because of the broadening of many of the JAZ ZF1 backbone resonances in the presence of RNA (Figure 4C). The presence of exchange broadening implies that the binding of ZF1 to the RNA is actually tighter (slower off-rate) than that of ZF2 or ZF3; the affinity of JAZ ZF1 for VAImin RNA could therefore be estimated by isothermal titration calorimetry (ITC) measurements (Figure 6). The data could only be reliably fit using a one-site binding model with a K_d = 23 ± 4 μM and a JAZ ZF1/RNA stoichiometric ratio of 2:1. This dissociation constant is only an approximation of the K_d value because interactions with the secondary binding site contribute to the measured heat of interaction. It was not possible to collect data points at higher molar ratios using ITC in order to fit using a two-site model because of the solubility limitations of the JAZ ZF1–RNA complex. Attempts to measure the dissociation constants of JAZ ZF23 with VAImin and a 30 bp Watson–Crick base-paired RNA using ITC were unsuccessful because of multimeric binding that prevented the calculation of K_d values for the complexes. Representative traces are shown in Figure S5. These results are consistent with the EMSA results (Figure 2), which show clearly that JAZ ZF12 and ZF23 bind RNA with nanomolar C_{50}'s in a multimeric fashion.

Mapping of the RNA Binding Sites on JAZ Zinc Fingers by NMR. Backbone-resonance assignments were made for all four of the single zinc finger JAZ constructs. Almost complete assignments could be made for JAZ ZF2 and ZF3, but the assignments for JAZ ZF1 were less complete because of resonance overlap in the center of the spectrum. Assignments for JAZ ZF4 were incomplete because of exchange broadening of cross peaks in the triple-resonance experiments used to assign ZF34. Assigned $^{1}H-^{15}N$ HSQC spectra for the single zinc finger proteins are shown in Figure S6.

The RNA binding sites on ZF1, ZF2, and ZF3 were identified from assigned HSQC cross peaks that shift and/or broaden in the presence of RNA. We find that the protein resonances that are perturbed by addition of RNA correspond to elements of the JAZ zinc fingers that are predicted to be structured, according to sequence homology with the known structures[15] of ZFa fingers. None of the observations made so far on dsRBP proteins, derived either from JAZ or ZFa, suggest that the linker regions interact directly with the RNA.

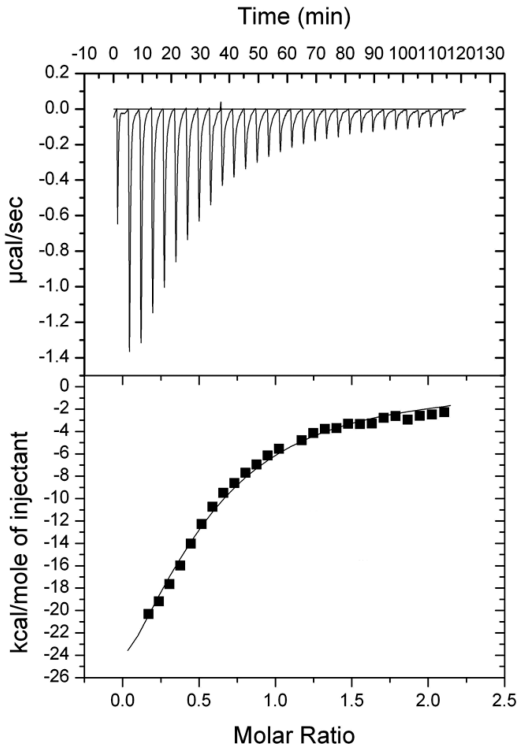

Figure 6. ITC titration of JAZ ZF1 with VAImin RNA. The curve in the lower panel is fitted to the experimental points using a model with 2:1 ZF/RNA.

NMR Solution Structure of JAZ ZF3. A set of 20 low-energy solution structures (Figure 7A) was calculated for JAZ ZF3 using CYANA 2.1,[40] refined by AMBER 9 incorporating a generalized-Born (GB) continuum solvent model,[31,32] and

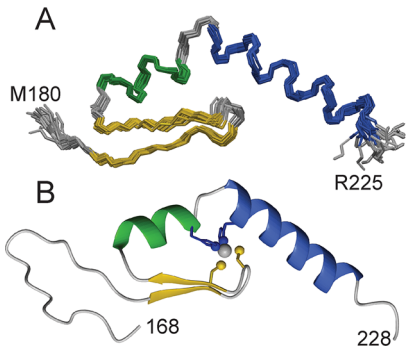

Figure 7. (A) Backbone ensemble of the well-structured region (residues 180–225) of the 20 lowest-energy NMR structures of JAZ ZF3. (B) Ribbon representation of the lowest-energy structure of JAZ ZF3, showing the secondary structural elements and the disordered N-terminal tail (residues 168–179). β-strands β1 and β2 are shown in gold, α1, in green, and α2, in blue. The zinc is shown as a gray sphere coordinated to the side chains of C187 and C190 (yellow) and H203 and H209 (blue). Figure made with Molmol.[58]

dx.doi.org/10.1021/bi401675h | *Biochemistry* 2014, 53, 1495–1510

included restraints for the zinc coordination as described previously[15] to the side chains of residues 187, 190, 203, and 209. A $^{15}N-^{1}H$ HMQC spectrum (Figure S7) shows that the zinc is coordinated by the Nε2 of H203 and by the Nδ1 of H209, as was observed for the ZFa zinc fingers.[15] Statistics for the ensemble of the 20 lowest-energy NMR structures of JAZ ZF3 are reported in Table 2.

Table 2. Structural Statistics for JAZ ZF3[a]

NMR Constraints	
total unambiguous distance restraints	209
intraresidue (i, i)	54
sequential (i, i + 1)	74
medium range ($2 \leq \lvert i - j \rvert \leq 4$)	33
long range ($\lvert i - j \rvert > 4$)	48
total dihedral angle restraints	77
Φ	38
Ψ	39
$\chi 1$	0
Ensemble Statistics	
Violation Analysis	
maximum distance violation (angstroms)	0.19
maximum dihedral angle violation (degrees)	0
Energies	
mean restraint violation energy (kcal mol^{-1})	2.5
mean AMBER energy (kcal mol^{-1})	−1880.4
Deviation from Idealized Geometry	
bond lengths (angstroms)	0.01
bond angles (degrees)	2.5
rmsd from mean structure	0.43
rmsd for all heavy atoms	1.04
Ramachandran Plot	
most favorable regions (%)	89.6
additionally allowed regions (%)	10.4
generously allowed regions (%)	0
disallowed regions (%)	0

[a]rmsd values and Ramachandran statistics are given for structured regions (residues 181 to 222) only.

Human JAZ ZF3 (residues 168−227) is structured from I181 to Y222 as defined by the presence of $^{1}H-^{13}C$ and $^{1}H-^{15}N$ NOEs and TALOS+ torsion-angle restraints (Figure 7). JAZ ZF3 adopts a $\beta\beta\alpha\alpha$ fold very similar to those of ZFa ZF1 and ZF2.[15] At the N-terminus is an antiparallel β-hairpin (residues K185−F194); the two β-strands are connected by a type I turn. A short structured loop (residues N195 and D196) connects the β-hairpin to the helix−kink−helix motif, with helix α1 spanning residues P197−V205 and helix α2, residues K208−Y222. Two relatively well-structured residues before the N-terminal β-strand (I181 and D182) appear to pack against the loop at the N-terminus of the α1 helix (D196 and P197). The zinc ligands of JAZ ZF3 are C187 in the first strand, C190 in the turn, H203 at the end of helix α1, and H209 at the beginning of helix α2. Hydrophobic residues (F194 and Y204) participate in packing interactions, but there is no well-defined hydrophobic core in JAZ ZF3, which, like ZFa,[15] requires the presence of zinc to form a folded structure. The surface of JAZ ZF3 is positively charged (pI = 9.3) because of the presence of numerous surface-exposed lysines (K207, K208, K211, K215, and K217) and arginines (R210 and R221) in the helix−kink−helix motif. A comparison of the changes in chemical shift as dsRNA is added to JAZ ZF3 and to ZFa ZF1 is shown in Figure 8A,B. These changes are mapped onto the backbones of the two zinc finger structures in Figure 8C. The similarity between the two zinc finger structures and their structural perturbations and RNA-binding surfaces, as revealed by the location of chemical-shift changes upon addition of RNA, is consistent with the high sequence homology between the structured regions of the two proteins.

Modeling of the JAZ ZF3−VAImin RNA Complex. The complex between JAZ ZF3 and a 19 base pair dsRNA, VAIminMut (Figure 4C, S2), was modeled using the program HADDOCK[19] utilizing backbone chemical-shift perturbation data from NMR titrations as ambiguous interaction restraints together with general information on protein-binding sites on RNAs.[19,41−43] No intermolecular NOEs for the JAZ ZF3−VAImin RNA complex were observed, likely because of the intermediate exchange observed in the HSQC spectra. Our EMSA and NMR results indicate that binding to the dsRNA does not depend on the base sequence of the RNA so that we are unable to define a preferred binding site for the JAZ fingers on RNA. Input data for the HADDOCK calculation therefore used only solvent-exposed residues with significant chemical-shift perturbations (≥0.9 times the standard deviation from the trimmed mean of the weighted average of ^{1}H and ^{15}N shift changes) as residue-level ambiguous interaction restraints for the protein, but it included all (except terminal) nucleotides in the RNA, consistent with the assumption that the JAZ zinc fingers could bind at multiple sites on the surface of the A-form RNA helix. The HADDOCK modeling program then allows any of the atoms from each residue designated as an ambiguous interaction restraint to interact with the dsRNA-binding partner. The entire A-form helix (minus the termini) was used to create a solvent-exposed interaction surface, allowing the protein to interact with any set of ≤17 bp in the RNA duplex. Models of the JAZ ZF3−VAIminMut RNA complexes were generated by docking the lowest-energy NMR structure of JAZ ZF3 to the idealized A-form VAIminMut RNA structural model.

When superimposed along the protein backbone, the HADDOCK models of the JAZ ZF3−RNA complex converge to form an ensemble of complexes in which the kink of the helix−kink−helix motif of JAZ ZF3 interacts with the RNA backbone centered on and directed toward the major groove (Figure 9A). When the same structures are superimposed along the RNA backbone (Figure 9B), the binding site of JAZ ZF3 is seen to vary between the structures: it is disordered with respect to rotation about the long axis of the duplex. Nevertheless, in all structures, JAZ ZF3 spans the major groove, making contacts with the phosphate backbone and the adjacent minor groove (Figure 9C, D). The interaction between JAZ ZF3 and dsRNA appears to be driven largely by the electrostatics and morphology of the A-form helix. The helix−kink−helix motif of JAZ ZF3 contains a number of arginine and lysine residues, which create a highly positively charged surface that accommodates the phosphate groups of the RNA backbone. The charge of the helix−kink−helix motif is augmented by the dipole of the α2 helix. The models suggest that positively charged residues of the helix−kink−helix motif, such as the side chains of K207, K208, K211, and K215 of JAZ ZF3, make multiple contacts with the phosphate backbone of the RNA and with riboses in the minor groove. In addition, the amide proton of K207 makes a hydrogen bond to the phosphate group of a guanine (Figure 9C). Both the interaction and the guanine appear to be conserved between the structures

dx.doi.org/10.1021/bi401675h | Biochemistry 2014, 53, 1495−1510

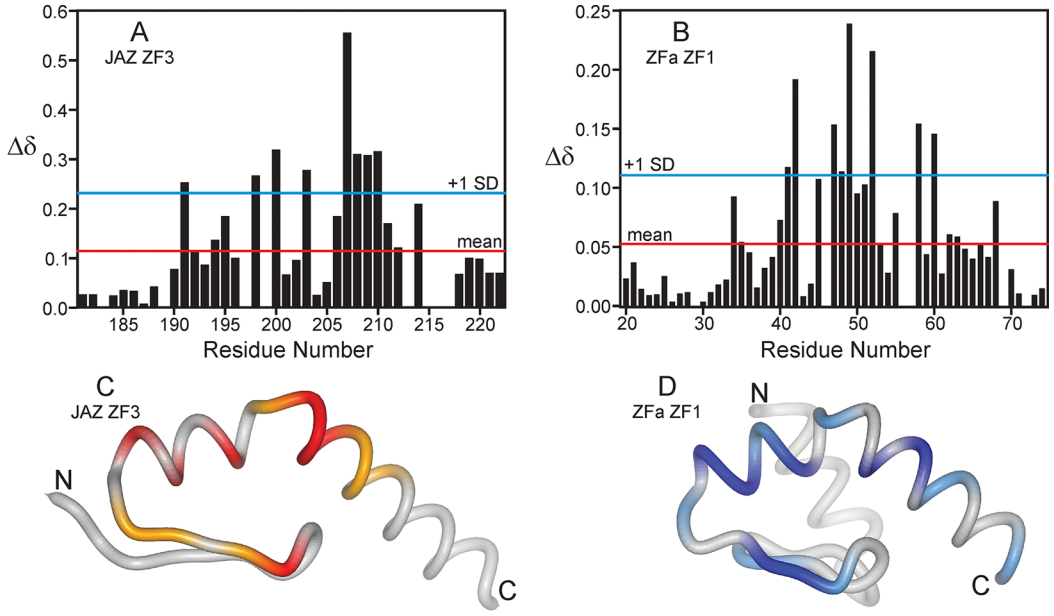

Figure 8. (A, B) Perturbation of the backbone amide (^{1}H and ^{15}N) resonances of (A) JAZ ZF3 and (B) ZF1 of the homologous protein ZFa. $\Delta\delta = [(\Delta\delta_{HN})^2 + (\Delta\delta_N/5)^2]^{1/2}$. Red horizontal lines indicate the average $\Delta\delta$ (0.115 for JAZ ZF3 and 0.053 for ZFa ZF1), and blue lines indicate [average + 1× standard deviation] (0.122 for JAZ ZF3 and 0.056 for ZFa ZF1). (C, D) Backbone representation of the lowest-energy structures from the ensembles of (C) JAZ ZF3 and (D) ZFa ZF1.[15] Residues for which $\Delta\delta$ > [average + 1× standard deviation] are colored red and blue for JAZ ZF3 and ZFa ZF1, respectively, and residues for which [average + 1× standard deviation] < $\Delta\delta$ < [average] are colored orange and light blue for JAZ ZF3 and ZFa ZF1, respectively. ZFa ZF1 has an extension (light gray) at the N-terminus consisting of a third helix and a third β-strand.[15] Disordered residues at the termini have been omitted from the representation of both structures. Figure made with Molmol.[58]

of ZF3–RNA and IPTase–tRNA.[17] A comparison of the structures of JAZ ZF3 and the IPTase zinc finger protein from the tRNA complex is shown in Figure S8.

DISCUSSION

Multiple Complexes in the EMSA Experiments. The EMSA experiments of Figure 2 show the presence of multiple complexes of JAZ with RNAs of various sizes. This circumstance complicates the analysis of these data for quantitative estimates of the affinities. A qualitative estimate is given by the C_{50}, which is related only to the protein concentration at which half of the RNA has disappeared from the free-RNA position on the gel regardless of what state it has subsequently entered. It is the semiquantitative figure C_{50} that is used to inform on the relative affinities shown in Table 1. Using C_{50} as an estimate of binding affinity, we were able to define both minimal RNA and protein constructs for a structural study of the JAZ–RNA complex.

The formation of a number of complexes of different molecular weights as JAZ protein is added to the RNA is most likely because of the binding of the protein at multiple sites on the RNA, with each of these sites having comparable but slightly different affinity. More bands are observed in the gels for the two-finger constructs compared to ZF1–4, both for full-length VAI (Figure 2A) and for smaller RNAs (Figures 2B and S1), likely because of the higher stoichiometric ratio at which the two-finger proteins saturate all of the binding sites on the RNA. Higher-order RNA–protein complexes may also be attributable to bridging complexes in which two or more zinc fingers from one JAZ molecule interact with multiple RNA helices.

Does JAZ Have Any Specificity for RNA Sequence or Structure? The general consensus in the literature is that JAZ and its homologues Wig1 and ZFA have no identifiable sequence specificity for RNA binding, although they are all specific for binding to dsRNA (and to a lesser extent, DNA–RNA hybrids) and not to ssRNA or DNA. It has been suggested that dsRBZFP–RNA interactions may be determined primarily by the shape of the A-form helix,[12,16] yet a number of target RNA molecules have been specifically identified for JAZ, including the viral associated RNAI (VAI) RNA from adenovirus[10] and cellular dsRNA.[44] These molecules contain stretches of base-paired nucleotides, both Watson–Crick and non-Watson–Crick, as well as bulges, unpaired nucleotides, loops, and single-stranded overhangs. By examining the nucleotide sequences of the known targets of JAZ, we identified a series of possible RNA structural elements that could be tested to determine whether they were important components of the binding affinity of JAZ zinc fingers for RNA and hence could be identified as specificity features.

Examination by EMSA and NMR shows conclusively that there is very little effect of any of the irregularities in RNA structure on the affinity of JAZ for RNA. Quantitation of binding data is quite problematic for this system because of multimeric and heterogeneous binding between the JAZ zinc fingers and RNA. However, the RNA constructs where loops, bulges, and overhangs were systematically removed from the target VAI RNA showed very little difference in affinity for the JAZ zinc fingers. The finding that 3′ overhangs are not recognized by JAZ is surprising because it has been suggested that Wig-1 recognizes overhangs in a 21 bp RNA.[13] The JAZ zinc fingers bind equally well to a cellular dsRNA, pre-miR34a, as to viral dsRNA. We conclude that the presence of A-form RNA, with or without minor defects because of noncanonical base pairing, is all that is required for binding to JAZ zinc fingers. The only requirement appears to be the presence of a minimal length of well-structured RNA that adopts an A-form helix of sufficient length to provide sites for binding. We have

dx.doi.org/10.1021/bi401675h | Biochemistry 2014, 53, 1495–1510

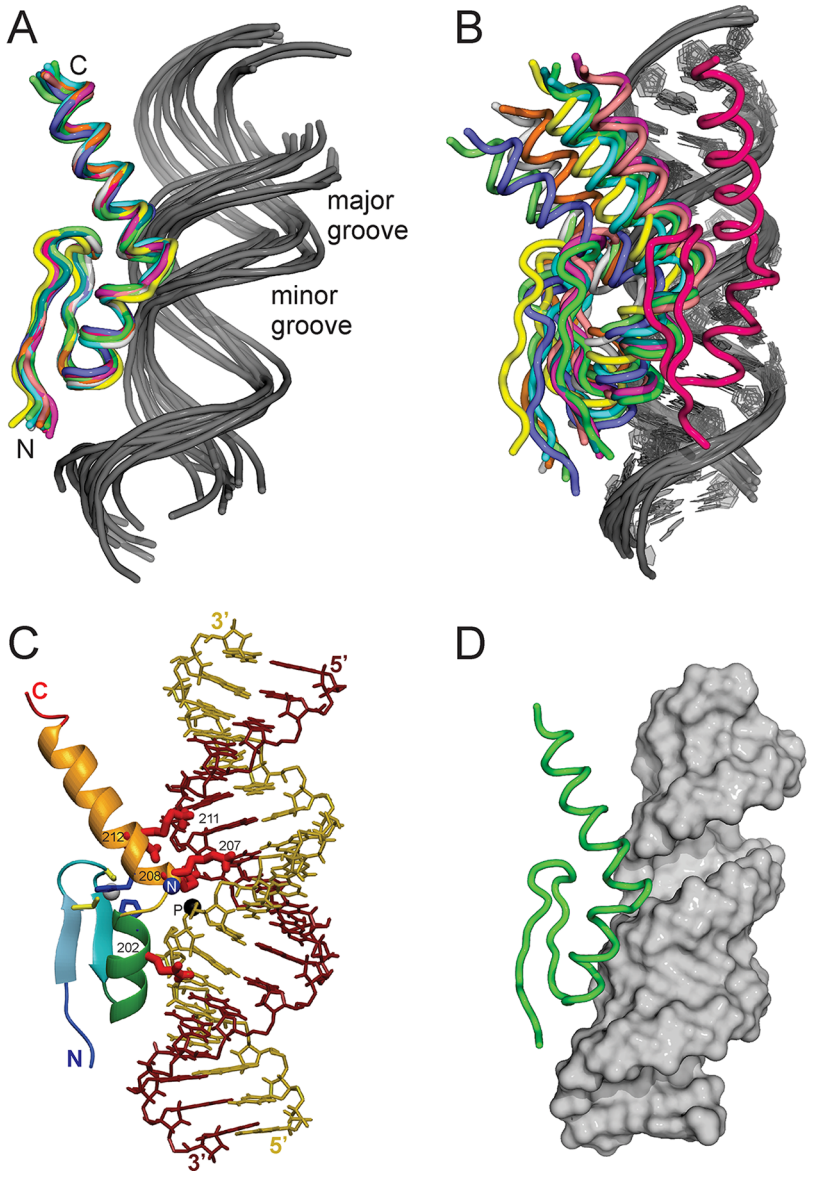

Figure 9. (A, B) Models of the complex between JAZ ZF3 and the minimal dsRNA VAIminMut shown (A) superimposed on the structured portions of the backbone of ZF3 and (B) superimposed on the backbone of the dsRNA duplex. (C) Model of the complex between ZF3 and the minimal dsRNA showing interactions between the side chains of Q202, K207, K208, K211, and Q212 (shown in red) with the phosphate backbone of the RNA. The backbone amide of K207 (blue sphere) and the phosphorus of Cyt13 (black) are shown in close proximity in the complex. (D) Single HADDOCK model with the dsRNA shown in a surface representation, illustrating the docking of the JAZ ZF3 in the major groove. Figure made with (A, B, D) PyMol and (C) Molmol.[58]

identified a minimal length of RNA, VAImin, which was subsequently used to characterize the binding of individual JAZ zinc fingers using NMR. Preferential binding of dsRNA over dsDNA by JAZ ZF3 (Figures 3 and S4) provides further evidence that the A-form RNA conformation is fundamental to nucleic acid recognition by JAZ ZF3. Our data confirm previous findings that showed JAZ and ZFa preferentially bind to A-form over B-form helices.[10,12]

Results from EMSA experiments and NMR titrations indicate that the binding affinity of JAZ zinc fingers for RNA is dependent on the length of the A-form helix. Quantitative NMR titrations of JAZ ZF3 with VAImin RNA show that dsRNA with approximately 17 base pairs provides two binding sites, with K_{d1} of the order of 10 μM and K_{d2} of the order of 100 μM, which are each occupied by one zinc finger domain. We believe that the K_d's differ because the binding of the proteins is negatively cooperative. The protein binding sites on the RNA are in close proximity; after the binding of the first protein, the affinity of the second protein is reduced, likely because of charge-neutralization effects. In essence, the first K_d is measuring the affinity of the protein for the RNA, which is relatively high, whereas the second K_d is measuring the affinity of the protein for an RNA−protein complex.

ITC and quantitative NMR titration experiments indicate that JAZ ZF1, ZF2, and ZF3 have similar binding affinities for VAImin RNA and that the 2:1 (ZF/RNA) stoichiometry of the complex is conserved. Spectra of the imino-proton resonances of VAImin RNA show this RNA remains in an A-form conformation when bound to JAZ ZF2 or JAZ ZF3.

Role of Multiple Zinc Fingers in RNA Binding. The RNA-binding affinity estimated by C_{50} values of full-length JAZ (ZF1−4) is higher than that of one- or two-finger constructs.

dx.doi.org/10.1021/bi401675h | *Biochemistry* 2014, 53, 1495−1510

Affinity for RNA is weakest in constructs with only one RNA-binding zinc finger, ZF1, ZF2, and ZF3, and the two-finger construct ZF34. EMSA results demonstrate that the RNA-binding affinity of the two-finger JAZ constructs, and the respective stoichiometric ratios of their RNA−protein complexes depend on the number of active RNA-binding zinc finger domains they contain (i.e., ZF1−4 > ZF12 ≈ ZF23 > ZF34). JAZ ZF1−4 produces larger gel shifts compared to those of JAZ ZF12 and JAZ ZF23, consistent with the increased mass of JAZ ZF1−4 (more than twice that of the two-finger constructs).

Our NMR results that show that residues corresponding to the linker regions between fingers do not interact with RNA directly suggest that these nonconserved unstructured regions act to increase the RNA affinity only through a proximity effect, tethering the zinc fingers and increasing the effective local concentration of the zinc finger domains. This behavior is unlike that of the sequence-specific dsRBDs of PKR in which the linkers interact directly with their partner dsRNAs.[45−47] Other zinc finger proteins utilize linker regions to provide additional site-specific affinity through protein−protein interactions in binding RNA[48] or DNA,[49,50] a phenomenon that we have termed a *snap-lock*.[51] Interestingly, the absence of interfinger and finger-linker interactions as well as any evidence of contact between dsRNA and the linkers is a hallmark of the dsRBZFP proteins, both JAZ (this work) and ZFa,[15] and may be correlated with the complete absence of sequence specificity for their RNA targets.

Affinities of the dsRBP Zinc Fingers for dsRNA. Studies of the homologous proteins JAZ, ZFa, and Wig1 as well as mutagenesis experiments on JAZ suggested that all four of the JAZ zinc finger domains have dsRNA-binding activity.[10] Our EMSA and NMR studies show that JAZ ZF1, ZF2, and ZF3 all bind A-form dsRNAs with comparable affinity, whereas JAZ ZF4 does not interact at all with RNA. The absence of RNA binding by ZF4 is puzzling. JAZ ZF4 is highly homologous to the RNA-binding zinc fingers of JAZ and ZFa.[15] In particular, ZF4 has a sequence almost identical to those of ZFa fingers 4, 5, 6, and 7,[15] whereas the homology is much weaker between this set of fingers and ZF1, 2, and 3 of either of the two proteins (Figure 1A). A comparison of the RNA-binding properties of the N-terminal and C-terminal ZFa fingers[12] suggested that the modes of binding of ZFa ZF1−3 differed in a qualitative sense from the binding of ZFa ZF4−7 or ZF3−7. In particular, the apparent binding constants reported by Finerty and Bass[12] for full-length ZFa and for ZFa ZF1−3 are almost equivalent (0.5 nM), whereas the values reported for ZFa ZF4−7 (8.4 nM) and ZFa ZF5−7 (9.0 nM) are more than an order of magnitude weaker. These binding data suggest that ZFa ZF5, 6, and 7 have significantly lower affinities for dsRNA than ZFa ZF1, 2, or 3. The presence of ZFa ZF4 appears to have a negligible effect on the affinity in the context of multifinger constructs.[12] This observation seems to imply that ZFa ZF4, like JAZ ZF4, is not one of the primary binding sites for dsRNA. Finerty and Bass[12] suggest, on the basis of the difference in affinity of the N-terminal and C-terminal zinc fingers of ZFa, that these regions of the protein may bind to different forms of dsRNA or alternatively may bind in a different manner. Our results likewise suggest that JAZ ZF4 may have a different function in the protein, perhaps to bind to different types of nucleic acid or possibly to other proteins. Amide resonances, largely for the α-helix and flexible loop regions, are broadened in the $^{1}H-^{15}N$ HSQC spectrum of JAZ ZF4. Structural modeling using CSRosetta[52] revealed that the C-terminus of ZF4 did not form α-helical structure and that this region was apparently random coil.

A detailed comparison of the particular residues that differ between the first three zinc fingers of ZFa and JAZ on the one hand and the last four fingers of ZFa and ZF4 of JAZ on the other reveals that the conserved sequence HYxx**K**KHK, which spans the helix−kink−helix motif in ZFa ZF1−3[15] and JAZ ZF1−3 (this work), is subtly changed in JAZ ZF4 (to HVSG**F**KHK) and ZFa ZF4−7 (to HISG**A**KHK). The replacement of the positively charged side chain of K by F (or A) may be sufficient to lower the RNA affinity of these zinc finger domains. Another potential substitution that could disrupt RNA binding is the presence of a glutamic acid at position 252 of JAZ ZF4 at a position analogous to V198 of JAZ ZF3 (and also present at this position throughout ZFa ZF4−7 (Figure 1B)). This residue shows significant chemical-shift changes as VAImin RNA is added to ZF3 and appears in the HADDOCK models as a prominent RNA contact site.

Biological Role of JAZ. Our binding studies also shed light on the molecular biology of JAZ. Although JAZ is thought to participate in the nucleocytoplasmic shuttling of pre-miRNA via the exportin pathway,[3] an interaction between JAZ and a pre-miRNA has not previously been reported *in vitro*. Our work provides the first report of a dsRNA-binding zinc finger protein interacting with a pre-miRNA of known function. The finding that JAZ ZF34 can bind to adenoviral VAI and human pre-miR34a dsRNAs with similar apparent affinities suggests that JAZ cannot distinguish between endogenous or exogenous dsRNAs. This is consistent with published data suggesting that for a protein to bind differentially to pathogenic dsRNA or endogenous dsRNA it must be capable of recognizing either specific RNA sequences or structural elements.[53−55] Our results suggest that JAZ, specifically zinc fingers 1, 2 and 3, is able to bind and decorate any dsRNA with at least 17, not necessarily canonical Watson−Crick, base pairs with moderate-to-high affinity.

Our results are consistent with the known role of JAZ in the transport of small double-stranded RNAs to and from the nucleus via the exportin-5 pathway.[3] For such a role, it makes sense that a transport-facilitating protein such as JAZ should have quite a modest affinity for the substrate, with no sequence specificity. This renders JAZ unable to discriminate between endogenous RNA sequences and pathogenic viral sequences, all of which are shuttled out of the nucleus into the cytoplasm to perform their biological functions. Clearly, JAZ has not evolved to discriminate between these RNA types and therefore forms no part of the defense of the cell against infection. In fact, JAZ appears to be a weak point in the antiviral defense system of cells. The hijacking of the cell's machinery by overwhelming it with exogenous biomolecules that mimic and out-compete their endogenous counterparts is a common method for viruses to gain ascendancy on the way to successful infection and viral reproduction (see, for example, ref 56). Understanding the methods by which this hijacking is achieved in important cellular systems may provide insights that will facilitate the design of new therapeutic approaches to disease.

The biological roles of dsRBZFP-like domains such as JAZ ZF4 that do not bind dsRNA remain unclear. Other dsRBD proteins that do not interact with RNA are often protein−protein interaction domains.[57] JAZ has been shown to interact with the tumor suppressor p53[14] and interleukin enhancer-binding factor 3.[3] Our studies confirm that JAZ ZF1, ZF2, and ZF3 bind to dsRNA. Sequence analysis[15] indicates that the

linkers between the zinc finger domains in JAZ are likely to be disordered, as they are in the homologous protein ZFa. It is tempting to speculate that a potential role for ZF4 of JAZ (together, perhaps, with some of the disordered linker regions) could be to act as a protein−protein interaction domain.

■ ASSOCIATED CONTENT

Supporting Information

EMSA gels for interactions between various nucleic acid and JAZ protein constructs, secondary structure models for all nucleic acid constructs, NMR spectra and ITC titrations for various single-finger JAZ constructs with RNA, and overlays of published structures of similar proteins with that of JAZ ZF3. This material is available free of charge via the Internet at http://pubs.acs.org.

■ AUTHOR INFORMATION

Corresponding Authors

*(H.J.D.) Tel.: 858-784-2223. Fax: 858-784-9822. E-mail: dyson@scripps.edu.

*(P.E.W.) Tel.: 858-784-9721. Fax: 858-784-9822. E-mail: wright@scripps.edu.

Present Address

†Freeslate, Inc., Sunnyvale California 94085, United States.

Funding

This work was supported by grant GM36643 from the National Institutes of Health and by the Skaggs Institute for Chemical Biology.

Notes

The authors declare no competing financial interest.

■ ACKNOWLEDGMENTS

We thank Joel Gottesfeld, Michael Summers, James Williamson, Gerard Kroon, Derrick Meinhold, Bethany Buck-Koehntop, and Donald Kerkow for helpful discussions and assistance, Peter Haberz for assistance with data fitting, and Martha Fedor, Joel Gottesfeld, and James Williamson for allowing us the use of their equipment and facilities for EMSA experiments.

■ ABBREVIATIONS USED

JAZ, just another zinc finger (also known as ZNF346); dsRNA, double-stranded RNA; tRNA, transfer RNA; ssRNA, single-stranded RNA; dsDNA, double-stranded DNA; dsRBD, dsRNA-binding domain; dsRBZFP, dsRNA-binding zinc finger protein; ZFa, zinc finger protein a; HSQC, heteronuclear single-quantum coherence; ZF, zinc finger domain; VAI RNA, adenovirus viral associated RNA I

■ REFERENCES

(1) Laity, J. H., Lee, B. M., and Wright, P. E. (2001) Zinc finger proteins: New insights into structural and functional diversity. *Curr. Opin. Struct. Biol. 11*, 39−46.

(2) Klug, A., and Rhodes, D. (1987) 'Zinc fingers': A novel protein motif for nucleic acid recognition. *Trends Biochem. Sci. 12*, 464−469.

(3) Chen, T., Brownawell, A. M., and Macara, I. G. (2004) Nucleocytoplasmic shuttling of JAZ, a new cargo protein for exportin-5. *Mol. Cell. Biol. 24*, 6608−6619.

(4) (2005) *Zinc Finger Proteins: From Atomic Contact to Cellular Function* (Iuchi, S., and Kuldell, N., Eds.) Kluwer Academic/Plenum Publishers, New York.

(5) Nicholson, A. W. (1996) Structure, reactivity, and biology of double-stranded RNA. *Prog. Nucleic Acid Res. Mol. Biol. 52*, 1−65.

(6) Saunders, L. R., and Barber, G. N. (2003) The dsRNA binding protein family: Critical roles, diverse cellular functions. *FASEB J. 17*, 961−983.

(7) Fierro-Monti, I., and Mathews, M. B. (2000) Proteins binding to duplexed RNA: One motif, multiple functions. *Trends Biochem. Sci. 25*, 241−246.

(8) Bernstein, E., Denli, A. M., and Hannon, G. J. (2001) The rest is silence. *RNA. 7*, 1509−1521.

(9) Lu, S., and Cullen, B. R. (2004) Adenovirus VA1 noncoding RNA can inhibit small interfering RNA and microRNA biogenesis. *J. Virol. 78*, 12868−12876.

(10) Yang, M., May, W. S., and Ito, T. (1999) JAZ requires the double-stranded RNA-binding zinc finger motifs for nuclear localization. *J. Biol. Chem. 274*, 27399−27406.

(11) Finerty, P. J., and Bass, B. L. (1997) A *Xenopus* zinc finger protein that specifically binds dsRNA and RNA-DNA hybrids. *J. Mol. Biol. 271*, 195−208.

(12) Finerty, P. J., and Bass, B. L. (1999) Subsets of the zinc finger motifs in dsRBP-ZFa can bind double-stranded RNA. *Biochemistry 38*, 4001−4007.

(13) Mendez-Vidal, C., Wilhelm, M. T., Hellborg, F., Qian, W., and Wiman, K. G. (2002) The p53-induced mouse zinc finger protein wig-1 binds double-stranded RNA with high affinity. *Nucleic Acids Res. 30*, 1991−1996.

(14) Yang, M., Wu, S., Su, X., and May, W. S. (2006) JAZ mediates G1 cell-cycle arrest and apoptosis by positively regulating p53 transcriptional activity. *Blood 108*, 4136−4145.

(15) Möller, H. M., Martinez-Yamout, M. A., Dyson, H. J., and Wright, P. E. (2005) Solution structure of the N-terminal zinc fingers of the *Xenopus laevis* double-stranded RNA-binding protein ZFa. *J. Mol. Biol. 351*, 718−730.

(16) Carlson, C. B., Stephens, O. M., and Beal, P. A. (2003) Recognition of double-stranded RNA by proteins and small molecules. *Biopolymers 70*, 86−102.

(17) Zhou, C., and Huang, R. H. (2008) Crystallographic snapshots of eukaryotic dimethylallyltransferase acting on tRNA: Insight into tRNA recognition and reaction mechanism. *Proc. Natl. Acad. Sci. U.S.A. 105*, 16142−16147.

(18) Andreeva, A., and Murzin, A. G. (2008) A fortuitous insight into a common mode of RNA recognition by the dsRNA-specific zinc fingers. *Proc. Natl. Acad. Sci. U.S.A. 105*, E128−E129.

(19) de Vries, S. J., van, D. M., and Bonvin, A. M. (2010) The HADDOCK web server for data-driven biomolecular docking. *Nat. Protoc. 5*, 883−897.

(20) Matt, T., Martinez-Yamout, M. A., Dyson, H. J., and Wright, P. E. (2004) The CBP/p300 TAZ1 domain in its native state is not a binding partner of MDM2. *Biochem. J. 381*, 685−691.

(21) Milligan, J. F., and Uhlenbeck, O. C. (1989) Synthesis of small RNAs using T7 RNA polymerase. *Methods Enzymol. 180*, 51−62.

(22) Lee, C. W., Arai, M., Martinez-Yamout, M. A., Dyson, H. J., and Wright, P. E. (2009) Mapping the interactions of the p53 transactivation domain with the KIX domain of CBP. *Biochemistry 48*, 2115−2124.

(23) Arai, M., Ferreon, J. C., and Wright, P. E. (2012) Quantitative analysis of multisite protein-ligand interactions by NMR: binding of intrinsically disordered p53 transactivation subdomains with the TAZ2 domain of CBP. *J. Am. Chem. Soc. 134*, 3792−3803.

(24) Shortle, D. (1996) The denatured state (the other half of the folding equation) and its role in protein stability. *FASEB J. 10*, 27−34.

(25) Johnson, B. A., and Blevins, R. A. (1994) NMRView: A computer program for the visualization and analysis of NMR data. *J. Biomol. NMR 4*, 603−614.

(26) Grzesiek, S., and Bax, A. (1992) Correlating backbone amide and side chain resonances in larger proteins by multiple relayed triple resonance NMR. *J. Am. Chem. Soc. 114*, 6291−6293.

(27) Grzesiek, S., and Bax, A. (1993) Amino acid type determination in the sequential assignment procedure of uniformly $^{13}C/^{15}N$-enriched proteins. *J. Biomol. NMR 3*, 185−204.

(28) Fesik, S. W., and Zuiderweg, E. R. P. (1988) Heteronuclear three-dimensional NMR spectroscopy. A strategy for the simplification of homonuclear two-dimensional NMR spectra. *J. Magn. Reson. 78*, 588−593.
(29) Shen, Y., Delaglio, F., Cornilescu, G., and Bax, A. (2009) TALOS+: A hybrid method for predicting protein backbone torsion angles from NMR chemical shifts. *J. Biomol. NMR 44*, 213−223.
(30) Güntert, P. (2004) Automated protein structure calculation with CYANA. *Methods Mol. Biol. 278*, 353−378.
(31) Case, D. A., Cheatham, T. E., III, Darden, T., Gohlke, H., Luo, R., Merz, K. M. J., Onufriev, A., Simmerling, C., Wang, B., and Woods, R. (2005) The Amber biomolecular simulation programs. *J. Comput. Chem. 26*, 1668−1688.
(32) Bashford, D., and Case, D. A. (2000) Generalized Born models of macromolecular solvation effects. *Annu. Rev. Phys. Chem. 51*, 129−152.
(33) Laskowski, R. A., Rullmann, J. A. C., MacArthur, M. W., Kaptein, R., and Thornton, J. M. (1996) AQUA and PROCHECK-NMR: Programs for checking the quality of protein structures solved by NMR. *J. Biomol. NMR 8*, 477−486.
(34) Kelley, L. A., and Sternberg, M. J. (2009) Protein structure prediction on the Web: A case study using the Phyre server. *Nat. Protoc. 4*, 363−371.
(35) Macke, T. J., and Case, D. A. (1998) in *Molecular Modeling of Nucleic Acids* (Leontis, N. B., and SantaLucia, J., Eds.) pp 379−393, American Chemical Society, Washington, DC.
(36) Schneider, R. J., Weinberger, C., and Shenk, T. (1984) Adenovirus VAI RNA facilitates the initiation of translation in virus-infected cells. *Cell 37*, 291−298.
(37) Chang, T. C., Wentzel, E. A., Kent, O. A., Ramachandran, K., Mullendore, M., Lee, K. H., Feldmann, G., Yamakuchi, M., Ferlito, M., Lowenstein, C. J., Arking, D. E., Beer, M. A., Maitra, A., and Mendell, J. T. (2007) Transactivation of miR-34a by p53 broadly influences gene expression and promotes apoptosis. *Mol. Cell 26*, 745−752.
(38) Zuker, M. (2003) Mfold web server for nucleic acid folding and hybridization prediction. *Nucleic Acids Res. 31*, 3406−3415.
(39) Jucker, F. M., Heus, H. A., Yip, P. F., Moors, E. H. M., and Pardi, A. (1996) A network of heterogeneous hydrogen bonds in GNRA tetraloops. *J. Mol. Biol. 264*, 968−980.
(40) Güntert, P., Mumenthaler, C., and Wüthrich, K. (1997) Torsion angle dynamics for NMR structure calculation with the new program DYANA. *J. Mol. Biol. 273*, 283−298.
(41) Dominguez, C., Boelens, R., and Bonvin, A. M. J. J. (2003) HADDOCK: A protein-protein docking approach based on biochemical or biophysical information. *J. Am. Chem. Soc. 125*, 1731−1737.
(42) de Vries, S. J., van Dijk, A. D., Krzeminski, M., van, D. M., Thureau, A., Hsu, V., Wassenaar, T., and Bonvin, A. M. (2007) HADDOCK versus HADDOCK: New features and performance of HADDOCK2.0 on the CAPRI targets. *Proteins 69*, 726−733.
(43) Volpon, L., D'Orso, I., Young, C. R., Frasch, A. C., and Gehring, K. (2005) NMR structural study of TcUBP1, a single RRM domain protein from *Trypanosoma cruzi*: Contribution of a beta hairpin to RNA binding. *Biochemistry 44*, 3708−3717.
(44) Gwizdek, C., Bertrand, E., Dargemont, C., Lefebvre, J. C., Blanchard, J. M., Singer, R. H., and Doglio, A. (2001) Terminal minihelix, a novel RNA motif that directs polymerase III transcripts to the cell cytoplasm. Terminal minihelix and RNA export. *J. Biol. Chem. 276*, 25910−25918.
(45) McKenna, S. A., Kim, I., Liu, C. W., and Puglisi, J. D. (2006) Uncoupling of RNA binding and PKR kinase activation by viral inhibitor RNAs. *J. Mol. Biol. 358*, 1270−1285.
(46) Kim, I., Liu, C. W., and Puglisi, J. D. (2006) Specific recognition of HIV TAR RNA by the dsRNA binding domains (dsRBD1-dsRBD2) of PKR. *J. Mol. Biol. 358*, 430−442.
(47) Ucci, J. W., Kobayashi, Y., Choi, G., Alexandrescu, A. T., and Cole, J. L. (2007) Mechanism of interaction of the double-stranded RNA (dsRNA) binding domain of protein kinase R with short dsRNA sequences. *Biochemistry 46*, 55−65.
(48) Lee, B. M., Xu, J., Clarkson, B. K., Martinez-Yamout, M. A., Dyson, H. J., Case, D. A., Gottesfeld, J. M., and Wright, P. E. (2006) Induced fit and "lock and key" recognition of 5S RNA by zinc fingers of transcription factor IIIA. *J. Mol. Biol. 357*, 275−291.
(49) Wuttke, D. S., Foster, M. P., Case, D. A., Gottesfeld, J. M., and Wright, P. E. (1997) Solution structure of the first three zinc fingers of TFIIIA bound to the cognate DNA sequence: Determinants of affinity and sequence specificity. *J. Mol. Biol. 273*, 183−206.
(50) Stoll, R., Lee, B. M., Debler, E. W., Laity, J. H., Wilson, I. A., Dyson, H. J., and Wright, P. E. (2007) Structure of the Wilms tumor suppressor protein zinc finger domain bound to DNA. *J. Mol. Biol. 372*, 1227−1245.
(51) Laity, J. H., Dyson, H. J., and Wright, P. E. (2000) DNA-induced α-helix capping in conserved linker sequences is a determinant of binding affinity in Cys_2-His_2 zinc fingers. *J. Mol. Biol. 295*, 719−727.
(52) Lange, O. F., Rossi, P., Sgourakis, N. G., Song, Y., Lee, H. W., Aramini, J. M., Ertekin, A., Xiao, R., Acton, T. B., Montelione, G. T., and Baker, D. (2012) Determination of solution structures of proteins up to 40-kDa using CS-Rosetta with sparse NMR data from deuterated samples. *Proc. Natl. Acad. Sci. U.S.A. 109*, 10873−10878.
(53) Nallagatla, S. R., Hwang, J., Toroney, R., Zheng, X., Cameron, C. E., and Bevilacqua, P. C. (2007) 5′-Triphosphate-dependent activation of PKR by RNAs with short stem-loops. *Science 318*, 1455−1458.
(54) Pichlmair, A., Schulz, O., Tan, C. P., Näslund, T. I., Liljeström, P., Weber, F., and Reis e Sousa, C. (2006) RIG-I-mediated antiviral responses to single-stranded RNA bearing 5′-phosphates. *Science 314*, 997−1001.
(55) Hornung, V., Ellegast, J., Kim, S., Brzozka, K., Jung, A., Kato, H., Poeck, H., Akira, S., Conzelmann, K. K., Schlee, M., Endres, S., and Hartmann, G. (2006) 5′-Triphosphate RNA is the ligand for RIG-I. *Science 314*, 994−997.
(56) Ferreon, J. C., Martinez-Yamout, M. A., Dyson, H. J., and Wright, P. E. (2009) Structural basis for subversion of cellular control mechanisms by the adenoviral E1A oncoprotein. *Proc. Natl. Acad. Sci. U.S.A. 106*, 13260−13265.
(57) Chang, K. Y., and Ramos, A. (2005) The double-stranded RNA-binding motif, a versatile macromolecular docking platform. *FEBS J. 272*, 2109−2117.
(58) Koradi, R., Billeter, M., and Wüthrich, K. (1996) MOLMOL: A program for display and analysis of macromolecular structures. *J. Mol. Graphics 14*, 51−55.

NOTE ADDED AFTER ASAP PUBLICATION

This paper was published ASAP on February 27, 2014 with an incorrect text cited in reference 18. The corrected version was reposted on March 3, 2014.